POLITECNICO DI TORINO
Repository ISTITUZIONALE

The PoliTO–UniRoma1 database of cyclic and dynamic laboratory tests: assessment of empirical predictive models

Original
The PoliTO–UniRoma1 database of cyclic and dynamic laboratory tests: assessment of empirical predictive models / Ciancimino, Andrea; Cosentini, Renato Maria; Foti, Sebastiano; Lanzo, Giuseppe; Pagliaroli, Alessandro; Pallara, Oronzo. - In: BULLETIN OF EARTHQUAKE ENGINEERING. - ISSN 1570-761X. - (2023). [10.1007/s10518-022-01573-y]

Availability:
This version is available at: 11583/2974602 since: 2023-01-13T13:48:27Z

Publisher:
Springer

Published
DOI:10.1007/s10518-022-01573-y

Terms of use:

This article is made available under terms and conditions as specified in the corresponding bibliographic description in the repository

Publisher copyright

(Article begins on next page)

12 October 2024

Bulletin of Earthquake Engineering
https://doi.org/10.1007/s10518-022-01573-y

ORIGINAL ARTICLE

The PoliTO–UniRoma1 database of cyclic and dynamic laboratory tests: assessment of empirical predictive models

Andrea Ciancimino[1] · Renato Maria Cosentini[1] · Sebastiano Foti[1] · Giuseppe Lanzo[2] · Alessandro Pagliaroli[3] · Oronzo Pallara[1]

Received: 21 April 2022 / Accepted: 19 November 2022
© The Author(s) 2023

Abstract
The soil nonlinear hysteretic behaviour is usually described, in the moderate strain range, through the shear modulus reduction and material damping ratio (MRD) curves. In common practice, in absence of specific laboratory tests, the curves are estimated by employing empirical regression models. Such predictive models, typically calibrated on large experimental datasets, correlate the soil response to its physical properties. This research fits within this context, presenting a comprehensive database of cyclic and dynamic laboratory tests conducted on natural Italian soils. The database, publicly available as supplementary data of the paper, contains the results of the tests conducted by the geotechnical laboratories of the Politecnico di Torino (Turin, Italy) and the *Sapienza* Università di Roma (Rome, Italy) over the past 30 years. The experimental data are employed to assess the performance of some widely used empirical models in predicting the MRD curves of natural uncemented fine-grained soils, emphasizing the importance of using an independent dataset for conducting a reliable statistical analysis. The results show that the use of many soil parameters as proxies for predicting the soil response does not necessarily lead to an improvement in the performance of the model. Therefore, according to Occam's razor principle, simple models are to be preferred.

Keywords Dynamic properties · Shear modulus · Damping ratio · Cyclic and dynamic tests · Empirical models · Database

List of symbols

A	Output amplitude
δ_{n+1}	Logarithmic decrement between two successive peak amplitudes in resonant column tests
D	Damping ratio

✉ Andrea Ciancimino
andrea.ciancimino@polito.it

[1] Department of Structural, Geotechnical and Building Engineering, Politecnico di Torino, Turin, Italy

[2] Department of Structural and Geotechnical Engineering, Sapienza Università di Roma, Rome, Italy

[3] Department of Engineering and Geology, Università degli Studi "G.d'Annunzio" Chieti-Pescara, Pescara, Italy

Published online: 12 January 2023

D_0	Small-strain damping ratio
D_s	Diameter of the specimen
$\overline{\varepsilon}$	Global normalized root-mean-square error
$\overline{\varepsilon}_{G_S/G_0}$, $\overline{\varepsilon}_D$	Normalized root-mean-square errors respectively for G_S/G_0 and D
e	Void ratio
e_i, e_c	Initial and after the consolidation void ratios
f	Loading frequency
f_0	First torsional resonance frequency of the sample in resonant column tests
f_1, f_2	Frequencies associated with an amplitude equal to $\sqrt{2}/2$ times the maximum one in resonant column tests
FC	Fine content
γ	Shear strain
γ_c	Cyclic shear strain amplitude
γ_{max}	Maximum shear strain in resonant column tests
γ_{tl}	Linear threshold shear strain
γ_{tv}	Volumetric threshold shear strain
G_0	Small-strain shear modulus
G_S	Secant shear modulus
H_s	Height of the specimen
I_θ	Mass polar moment of inertia of the specimen in resonant column tests
I_t	Driving system polar moment of inertia in resonant column tests
K	Coefficient of earth pressure
N	Number of loading cycles
OCR	Over-consolidation ratio
p'	Effective confining pressure
p_{atm}	Atmospheric pressure
PI	Plasticity index
θ_s	Maximum rotation of the sample in resonant column tests
ρ	Soil density
R^2	Statistical measure of the goodness-of-fit of the models
σ'_v	Vertical effective stress
τ	Shear stress
τ_c	Cyclic shear stress amplitude
u_w	Excess pore-water-pressure
V_s	Shear wave velocity
w_l	Liquid limit
w_p	Plastic limit
w_n	Natural water content
ΔW	Energy dissipated by the unit volume of soil within one loading cycle
W	Elastic energy stored by the unit volume of soil within one loading cycle
Y_i, $\hat{Y}_i$	Measured and predicted values of the ith dependent variable
$\overline{Y}$	Observed mean of the dependent variable
z_n, z_{n+1}	Successive peak amplitudes during the free vibrations in resonant column tests

1 Introduction

The response of soils to cyclic and dynamic loadings is characterized by pronounced nonlinearity, energy dissipation, degradation of mechanical properties with cycles and coupling between shear and volumetric strains. In engineering practice, such complex behaviour is conveniently described in the small-to-medium shear strain range referring to the equivalent linear viscoelastic parameters, namely the secant shear modulus G_S and the material damping ratio D. By considering an idealized shear stress–strain $\tau - \gamma$ cycle (Fig. 1), G_S is defined as the slope of the line connecting the edges of the loop, while D quantifies the amount of energy dissipated. The latter is typically computed in analogy with the equivalent viscous damping ratio of a single-degree-of-freedom system, as originally derived by Jacobsen (1930):

$$D = \frac{1}{4\pi}\frac{\Delta W}{W} \tag{1}$$

where: ΔW is the energy dissipated by the unit volume of the soil within one cycle, and $W = \gamma_c \tau_c / 2$ represents the elastic energy, being τ_c and γ_c the cyclic shear stress and strain amplitudes, respectively.

At very small strains, the material response is almost linear and, therefore, G_S is practically constant and equal to its initial, maximum, value G_0 (Hardin and Black 1968). Within this shear strain range, a small amount of energy is dissipated by the soil due to viscosity and friction between particles. The material thus exhibits a minimum, almost constant, small-strain damping ratio D_0 (e.g. Shibuya et al. 1995; Lanzo and Vucetic 1999). For γ_c larger than the linear threshold shear strain γ_{tl}, the nonlinear nature of soils becomes relevant and the dynamic parameters are typically described through the normalized modulus reduction G_S/G_0 and damping ratio D curves (hereafter, MRD curves), firstly introduced by Seed and Idriss (1970).

At large strains, the soil experiences a gradual degradation of the mechanical properties, resulting in either pore water pressure build-up or permanent changes in the

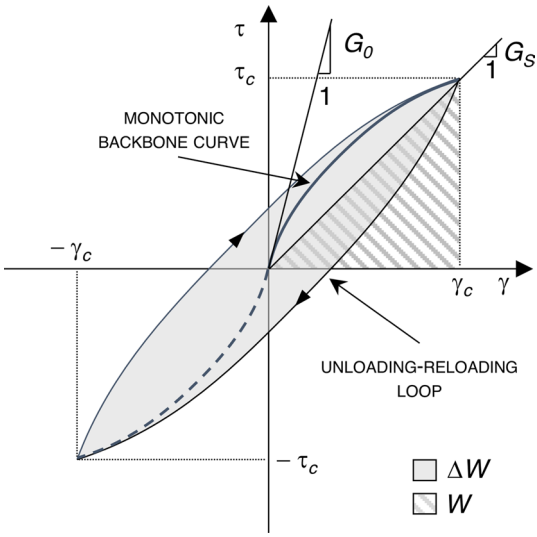

Fig. 1 Idealized stress–strain hysteretic loop

microstructure, depending on the drainage conditions (Silver and Seed 1971; Youd 1972; Stoll and Kald 1977). Such behaviour is typically associated with γ_c larger than the volumetric threshold shear strain γ_{tv} (Lo Presti 1991; Vucetic 1994).

The G_0 is known to be influenced by both physical properties—such as soil type, particle size distribution, and grain angularity—and state parameters usually expressed in terms of effective confining pressure p' and current void ratio e (e.g. Hardin and Black 1968; Kokusho et al. 1982; Menq 2003). In addition, the soil fabric and the stress history, usually expressed in terms of overconsolidation ratio, strongly affect the material's small-strain behaviour.

In absence of specific cyclic or dynamic laboratory tests conducted on the soil under consideration, it is possible to adopt empirical models to predict its nonlinear hysteretic response (e.g. Seed and Idriss 1970; Vucetic and Dobry 1991; EPRI 1993; Ishibashi and Zhang 1993; Darendeli 2001; Menq 2003; Zhang et al. 2005; Oztoprak and Bolton 2013; Ciancimino et al. 2020; Wang and Stokoe 2022). Such models, usually calibrated on databases of experimental data, allow for the estimation of the MRD curves based on some input parameters. As a consequence, several studies have been devoted in the past years to the development of large databases of experimental data (e.g., Vardanega and Bolton 2013; Wang and Stokoe 2022), some of them publicly available (e.g., the VEL project database, Giusti et al. 2021, and the Facciorusso 2021, archive). For fine-grained soils, the main input parameters are plasticity index PI, effective confining pressure p', over-consolidation ratio OCR, and the number of loading cycles N (Kokusho et al. 1982; Vucetic and Dobry 1991; Shibuya et al. 1995; Darendeli 1997; Lanzo et al. 1997; Lo Presti et al. 1997). Additionally, the loading frequency f is recognized to affect the response of fine-grained soils, as a consequence of its strain-rate dependency (e.g., Lo Presti et al. 1997; Tatsuoka et al. 2000; Matešić and Vucetic 2003; Mortezaie and Vucetic 2013). Such an influence is therefore connected to the PI of the material and, for a given soil, to the shear strain level (Lo Presti et al. 1997; Tatsuoka et al. 2000). For coarse-grained materials, particle size distribution and void ratio e also play a role (Seed et al. 1986; Menq 2003; Wang and Stokoe 2022).

Despite a large amount of research carried out in the past years on this subject, predicting the MRD of natural soils is still challenging (e.g. Kishida 2016; Ciancimino et al. 2019). This research intends to contribute to the discussion, providing insights regarding the use of empirical predictive models. To this aim, a wide database of cyclic and dynamic laboratory tests is assembled. The database comprises the results of tests conducted on natural, uncemented, Italian soils by the geotechnical laboratories of the Politecnico di Torino (hereafter PoliTO) and the *Sapienza* Università di Roma (hereafter UniRoma1) over the past 30 years. The data set, publicly available as supplementary data for this paper, also includes the physical properties of the investigated soils. It represents a significant resource for both scientific research and practical applications.

The testing procedures are firstly presented, along with the data interpretation methods. Then, after a general presentation on the structure and organization of the experimental data, a subset of the database is used to assess the performance of empirical models in predicting the nonlinear hysteretic behaviour of Italian soils. Specifically, the models considered are those proposed by: (1) Vucetic and Dobry (1991); (2) Darendeli (2001); (3) Ciancimino et al. (2020); and (4) Wang and Stokoe (2022). Statistical analysis is performed to highlight the abilities—and, potentially, the drawbacks—of the models based on reliable *independent* experimental data, which have not been used for calibrating these empirical relationships.

2 Testing procedures and data interpretation

The compiled dataset includes the results of cyclic and dynamic laboratory tests performed by PoliTO and UniRoma1. Specifically, Cyclic Double Specimen Direct Simple Shear (CDSDSS) tests were performed by UniRoma1, whereas Resonant Column (RC) tests were carried out by PoliTO. Although the tests were conducted over a long period, the main testing procedures, as well as the techniques employed to interpret the experimental results, remained consistent over the years.

2.1 Cyclic double specimen direct simple shear test

The CDSDSS tests were carried out using a modified version of the standard direct simple shear device developed by the Norwegian Geotechnical Institute (Bjerrum and Landva 1966). The double specimen configuration was specifically designed at the University of California in Los Angeles to overcome the issues associated with false deformations and system compliance which affects the measured soil response at small strains. The apparatus of the geotechnical laboratory of UniRoma1 was built based on the original prototype designed by Doroudian and Vucetic (1995). A full description of the experimental device can be found in D'Elia et al. (2003). It can investigate the soil cyclic response in a wide strain range, varying between 3×10^{-4}% and 7%, allowing it to measure both the small-strain parameters and the MRD curves (Lanzo et al. 2009).

In the framework of an International Round Robin Test, comparisons between CDSDSS and RC/TS tests were carried out on the undisturbed Italian Augusta clay, showing a very satisfactory agreement in terms of MRD curves (Cavallaro et al. 2003).

The tests are performed on saturated samples, consolidated up to the desired vertical effective stress σ'_v under pseudo-oedometric conditions owing to the lateral confinement exerted by wire-reinforced membranes. The samples are subjected to several steps of strain-controlled shearing cycles through a horizontal piston. Each step is generally constituted by 10 sinusoidal loading cycles, applied at the same shear strain amplitude γ_c with an almost constant frequency of 0.25 Hz. The cyclic shearing is applied under constant-volume conditions by preventing sample height variations. Such a procedure, firstly suggested by Bjerrum and Landva (1966), is practically equivalent to testing samples under fully undrained conditions (Dyvik et al. 1987).

The applied horizontal displacement and the corresponding horizontal force are used to compute the shear stress τ and strain γ, which describe the cyclic response of the material. Figure 2 shows the stress–strain cycles as measured from CDSDSS tests at increasing levels of γ_c. The figure refers to a test conducted on a sandy sample, for which typical S-shaped loops are observed at large strains (Fig. 2d). For each strain amplitude, G_S and D are directly inferred from the $\tau - \gamma$ loops (as shown in Fig. 1); in particular, the values employed in the analyses are obtained as the average of cycles n. 2–3–4 for each constant γ_c step.

2.2 Resonant column test

The RC tests were carried out using the free-fixed device of the geotechnical laboratory of PoliTO (Lo Presti et al. 1993, 1997). The apparatus can perform both resonant column or cyclic torsional shear tests, although in this paper reference is made only to RC tests. It is equipped with an electromagnetic driving system constituted of eight

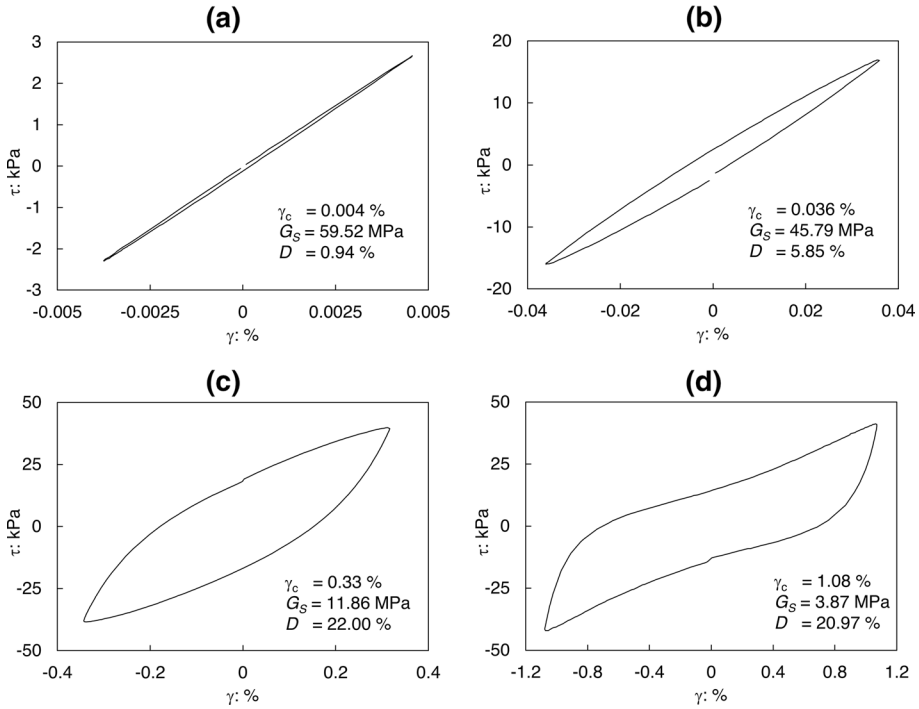

Fig. 2 Typical stress–strain $\tau - \gamma$ loops obtained from CDSDSS tests for increasing levels of cyclic shear strain amplitude γ_c

coils and four magnets (SBEL, Arizona). The motor can apply, under loading control, sinusoidal loading torques with a maximum amplitude of 1 Nm. The radial and axial strains are measured using proximity sensors. The soil response under dynamic loading conditions is tracked by an accelerometer mounted on the top of the specimen, whereas the sample rotation in torsional shear tests is measured by proximity transducers with targets integral to the driving system. Tests can be performed on both solid and hollow specimens, either isotropically or anisotropically consolidated. Nevertheless, the vast majority of the tests presented in the database were performed on solid specimens under isotropic conditions.

The samples are firstly saturated and consolidated up to the desired p'. The soil response is then investigated for γ_c ranging from 10^{-5}% to about 0.6% by applying cyclic torques with increasing amplitude. Specifically, a frequency sweep (typically a 40 Hz range with a frequency-step of 0.1 Hz) is applied for each loading amplitude to identify the resonance condition of the first torsional mode of the specimen. For each testing frequency, 20 cycles of forced vibrations are usually followed by 10 cycles of free vibrations (Fig. 3a). The amplitude, characteristic of the sample response under forced vibrations, is computed as the Root Mean Square (RMS) of the output amplitude A measured by the accelerometer. The computation is repeated for each loading frequency and the amplitude versus frequency curve is plotted to identify the first torsional resonance frequency of the sample f_0, corresponding to the maximum measured amplitude (Fig. 3b).

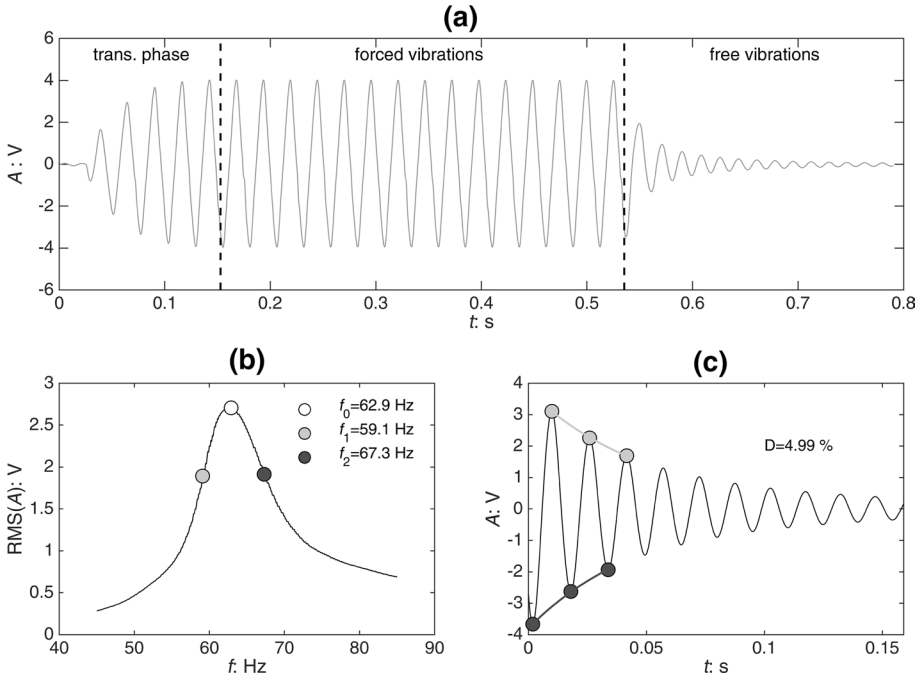

Fig. 3 Typical results of a RC test for a given loading amplitude: **a** time-history of the output amplitude A for one loading frequency; **b** amplitude A versus frequency f response curve; and **c** free-vibration decay method

Once obtained f_0, the shear wave velocity V_s is obtained via the theory of torsional waves propagation in a linear viscoelastic medium under steady-state conditions (Richart et al. 1970):

$$\frac{I_\theta}{I_t} = \frac{2\pi f_0 H_s}{V_S} \cdot \tan\left(\frac{2\pi f_0 H_s}{V_S}\right) \tag{2}$$

where I_θ is the mass polar moment of inertia of the specimen, I_t is the driving system polar moment of inertia and H_s is the height of the specimen. Based on the density of the soil ρ, the secant shear modulus G_S is thus computed as:

$$G_S = \rho \cdot V_S^2 \tag{3}$$

The reference cyclic shear strain amplitude γ_c is equal to 2/3 of the maximum shear strain γ_{max} (Hardin and Drnevich 1972). The latter can be computed, in a fixed-free device, as (Woods 1978):

$$\gamma_{max} = \frac{\theta_s \cdot D_s}{2 \cdot H_s} \tag{4}$$

where θ_s is the maximum rotation of the sample obtained by double integrating the angular acceleration defined through the accelerometer, while D_s and H_s are the diameter and the height of the specimen, respectively.

The damping ratio can be evaluated through either the half-power bandwidth or the free-vibration decay method. The former is based on the bandwidth of the amplitude versus frequency $A - f$ response curve (Fig. 3b). For relatively small D values, the equivalent viscous damping can be approximated by:

$$D = \frac{f_2 - f_1}{2f_0} \tag{5}$$

being f_1 and f_2 the frequencies associated with an amplitude equal to $\sqrt{2}/2$ times the maximum one (Fig. 3b).

The free-vibration decay method is instead applied considering the 10 cycles of free-damped vibrations at the end of the loading cycles (Fig. 3c). By knowing two successive peak amplitudes z_n and z_{n+1}, the logarithmic decrement δ_{n+1} is computed as:

$$\delta_{n+1} = \ln\left(\frac{z_n}{z_{n+1}}\right) \tag{6}$$

The average value δ is used to compute the damping ratio as:

$$D = \frac{\delta}{2\pi} \tag{7}$$

The two aforementioned methods were applied in most of the tests. For a few, old, tests D was instead obtained through the resonance factor method, based on the ratio between the output rotation amplitude at resonance to the pseudo-static rotation amplitude (Drnevich et al. 1978).

The electromagnetic driving system is known to be responsible for an additional small amount of equipment-generated damping (Cascante et al. 2003; Meng and Rix 2003; Wang et al. 2003), which is reduced if the input current is switched off, as during the free damped vibrations. Despite recent studies highlighting that D measurements are not excessively affected by this bias (e.g. Senetakis et al. 2015), measurements from the free-vibration decay were therefore preferred, when available, to data coming from steady-state vibration. Moreover, data obtained from the half-power bandwidth method were included only for γ_c amplitudes lower than 0.1%, due to the well-known limitations of the method in the large strain range.

3 Database of natural soils

The PoliTO–UniRoma1 database includes the results of cyclic and dynamic laboratory tests performed by the two Universities in the past 30 years. It comprises a total of 252 tests: 110 RC tests and 142 CDSDSS tests, carried out on natural soil samples. Figure 4 shows the spatial distribution of the investigated sites, with different markers according to the laboratory that has performed the test.

The database represents a reliable set of experimental results, suitable for conducting statistical analyses on the variability of the cyclic response of natural soils. The latter is particularly relevant given the growing attention of the scientific community towards the influence of uncertainties inherent in the MRD curves on the outcomes of ground response analyses (e.g. Bahrampouri et al. 2019; Aimar et al. 2020). Additionally, the experimental

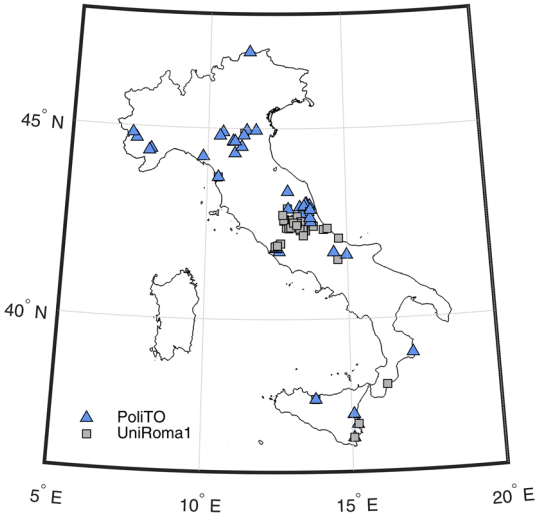

Fig. 4 Spatial distribution of sample locations

data can be used as reference values for practical applications, in absence of a specific characterization of the site.

3.1 Structure of the compiled dataset

The data are compiled in the form of a structured-variable, developed within the Matlab (2020) environment. The variable is available as open-access supplementary data for this paper. In addition, the data archive is also reported in a spreadsheet.

The structure of the database is presented in Fig. 5. Each test is identified with a unique "Sample ID" composed of a progressive number and an identifier of the laboratory that carried out the test (e.g., "006_POLITO"). The first field of the variable contains the "General information" about the samples in terms of site information (namely: the approximate location from which the sample was retrieved along with the sampling depth) and soil material type, as resulting from the Unified Soil Classification System (USCS, ASTM International 2017). When available, it is also reported the field small-strain shear modulus $G_{0,field}$ computed via Eq. (3) as a function of the field V_S of the soil, the latter being inferred through geophysical investigations.

The database includes information on the "Physical properties" of the tested materials. Specifically, it reports the unit weight, the main fractions coming from the Particle Size Distribution (PSD), the natural water content w_n, and the index properties of the samples, namely: the plasticity index PI, the liquid limit w_l, and the plastic limit w_p. It is worth mentioning that the information is incomplete for some tests. However, the database includes only materials for which at least PI is available, as it is recognized as the main parameter controlling the cyclic behaviour of natural fine-grained soils (Kokusho et al. 1982; Dobry and Vucetic 1987; Vucetic and Dobry 1991).

The results of cyclic and dynamic laboratory tests are stored in the "Testing data" field. The latter includes the initial and post-consolidation void ratios (e_i and e_c) along with either the effective confining pressure p' or the vertical stress σ'_v, respectively for RC and CDSDSS tests. When available, it is also reported the overconsolidation ratio OCR at which the test was performed. The experimental data are saved in the RC/CDSDSS

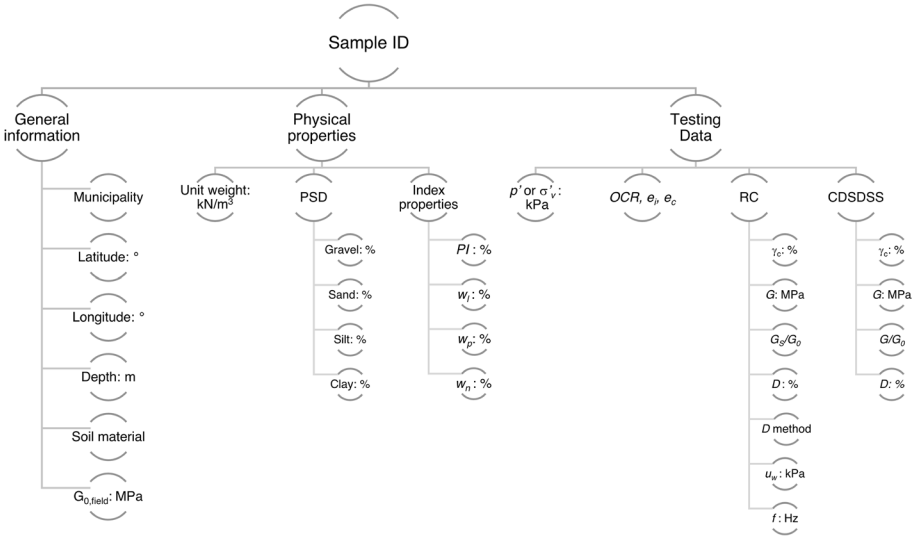

Fig. 5 Structure and organization of the database

subfield, according to the laboratory which has performed the test. For RC tests, the excess pore-water-pressure u_w and the testing frequencies f (which are instead almost constant and equal to 0.25 Hz for CDSDSS tests) are presented in addition to the MRD curves. Moreover, it is also reported the subfield "D method", which contains information on the experimental approach adopted for estimating the damping ratio.

"Appendix 1" contains general information about the compiled data, including sample ID, site information, soil type (when available) according to USCS (ASTM International 2017), PI, and p' or σ'_v (according to the type of test conducted).

3.2 Main characteristics of the investigated soils

The database comprises mainly the results of tests conducted on fine-grained soils, although some experimental data concerning the response of natural silty sands are also included. According to the Casagrande (Fig. 6a) and activity (Fig. 6b) charts, the fine-grained soils are mainly classifiable as low-to-normal active clays and silts. Only one of the investigated soils (red marker in Fig. 6) is very active silt, with a $PI = 122$.

Figure 7 reports the statistical distributions of the main characteristics of the investigated samples. The specimens were retrieved mainly from depths comprised between 0 and 30 m, whereas just 22% of the materials come from depths larger than 30 m. The 48% of the investigated soils are characterized by $15\% < PI < 30\%$, while the remaining materials are almost equally distributed between lightly ($PI < 15\%$) and highly ($PI > 30\%$) plastic soils. The laboratory tests were conducted at p' varying from 20 kPa to about 1100 kPa. For CDSDSS tests, p' is estimated based on σ'_v considering a coefficient of earth pressure $K = 0.5$. The corresponding $G_{0,lab}$ values, defined as the maximum G_S value measured in a given test, range from 7 to 341 MPa, despite the vast majority of the materials has $25\,\text{MPa} < G_{0,lab} < 200\,\text{MPa}$.

The G_0 is strongly dependent on the soil structure and the stress history. As a result, laboratory tests quite frequently lead to underpredicted (or, more rarely, overpredicted) G_0

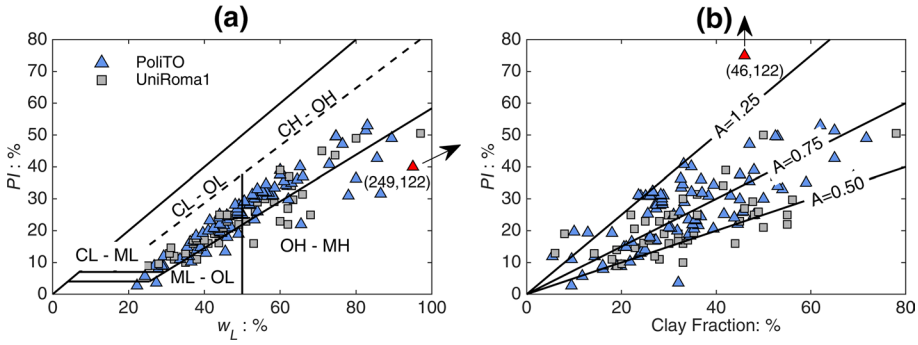

Fig. 6 Classification of the fine-grained soils according to **a** Casagrande and **b** activity charts. The actual position of the red triangle is defined by its coordinates within brackets

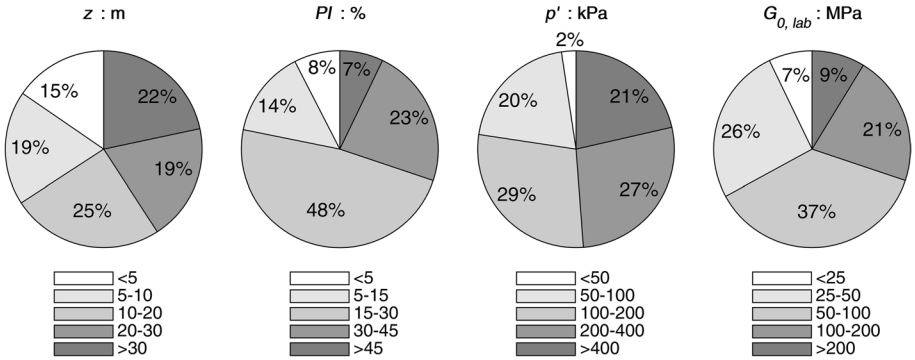

Fig. 7 Main characteristics of the compiled data

values compared to field measurements. As recognized by several studies, this laboratory underestimation is mainly due to sample disturbance effects (Anderson and Woods 1975; Stokoe and Santamarina 2000; Pagliaroli et al. 2014; Ciancimino et al. 2020). A comparison between the laboratory, $G_{0,lab}$, and the field, $G_{0,field}$, small-strain shear moduli is presented in Fig. 8 for 55 samples for which the laboratory tests were conducted at p' coherent with the in situ geostatic stress. It is quite evident that as the $G_{0,field}$ increases, the difference between $G_{0,field}$ and $G_{0,lab}$ also increases, shifting the points from the diagonal of the plot. In other words, the stiffer is the soil, the larger will be the sample disturbance effect. The latter is consistent with previous studies (e.g., Stokoe and Santamarina 2000; Pagliaroli et al. 2014), which highlighted the relevance of the sampling procedure on the soil small-strain response. Therefore, it is once again confirmed the best practice of measuring G_0 through field tests and then computing the G_S curve by multiplying the normalized G_S/G_0 curve measured in the laboratory by $G_{0,field}$.

3.3 Experimental results

The results of RC and CDSDSS tests are shown in Fig. 9 in terms of MRD of the investigated soils as a function of PI. The experimental data are in good agreement with

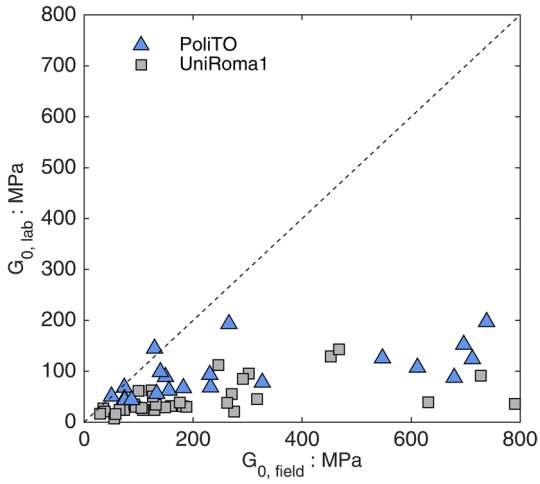

Fig. 8 Comparison between field and laboratory G_0 values

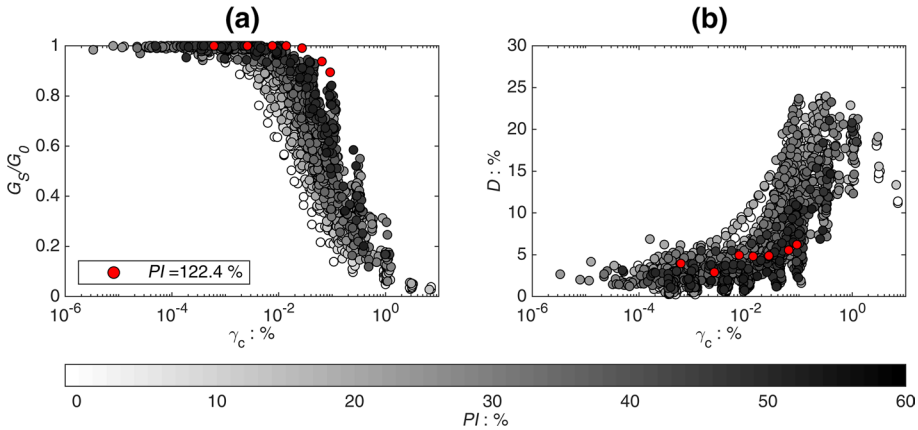

Fig. 9 Modulus reduction (**a**) and damping ratio (**b**) curves as a function of *PI*

previous findings (e.g. Vucetic and Dobry 1991; EPRI 1993; Darendeli 2001): the almost linear strain range tends to increase with increasing *PI*, shifting the nonlinear strain range towards larger γ_c (Fig. 9a); similarly, an increase of *PI* implies a slower increase of *D* with γ_c (Fig. 9b). In the small-strain range, soils characterized by large *PI* values usually show larger D_0. As a result, the *D* curves present a cross-over shear strain between about 10^{-4}% and 10^{-2}% consistent with previous experimental results (EPRI 1993; Stokoe et al. 1995; Lanzo and Vucetic 1999). The latter separates the small-strain field, where highly plastic soils show larger *D* values, from the nonlinear strain field.

The dependency of the nonlinear soil response from *PI* is highlighted in Fig. 10, which reports the linear γ_{tl} and the volumetric γ_{tv} shear strain thresholds of the samples contained in the database, with over imposed the trends obtained by Vucetic (1994). The γ_{tl} is here defined as γ_c corresponding to $G_S/G_0 = 0.99$ (after Vucetic 1994). The definition of γ_{tv} is instead more problematic, as no information is available about cyclic degradation and the pore-water pressure is monitored only during RC tests. Consequently, the γ_{tv} is obtained as the strain level

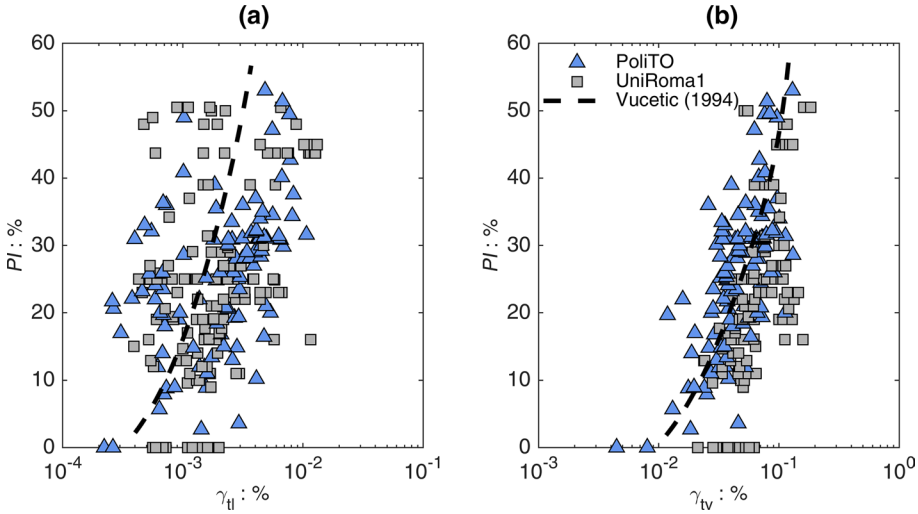

Fig. 10 Linear (**a**) and volumetric (**b**) shear strain thresholds as a function of *PI*

at the onset of the pore pressure build-up (i.e. $u_w/p' = 2\%$) for the RC tests, whereas it is equal to the γ_c corresponding to $G_S/G_0 = 0.65$ for the cyclic DSDSS tests. Such a criterion is defined based on the study by Vucetic (1994) confirmed also by Ciancimino et al. (2019), which suggested that G_S has to be reduced by approximately the 35% before that γ_{tv} is reached.

The data points are in good accordance with the trends defined by Vucetic (1994), highlighting an increase of both γ_{tl} and γ_{tv} with *PI* (Fig. 10). To put it in another way, highly plastic soils tend to show a larger practically linear strain range, shifting the nonlinear range towards larger γ_c. Conversely, sands and nonplastic silts tend to show a faster decay of the shear modulus and rapid degradation of their structure, leading to pore pressure build-up under undrained conditions. Such results are completely consistent with previous findings (e.g., Silver and Seed 1971; Youd 1972; Vucetic 1994; Tabata and Vucetic 2010; Mortezaie and Vucetic 2016), confirming also the quality of the compiled dataset.

The influence of p' is analyzed in Fig. 11, which presents the MRD curves obtained on soils with $15\% < PI < 25\%$. As recognized by previous studies (e.g., Seed and Idriss 1970; Ishibashi and Zhang 1993; Darendeli 2001; Zhang et al. 2005) an increase of p' implies a larger almost linear strain range and, in turn, a slower increase of D with γ_c. Nevertheless, it can be observed from Fig. 11 that its importance is limited for fine-grained soils. As also highlighted by Lanzo et al. (1997), the effect of p' on the MRD curves tends to vanish for medium to large plasticity soils.

4 Performance of empirical predictive models

Statistical analysis is conducted to investigate the performance of widely used empirical models in predicting the MRD curves of Italian soils. It is worth noting that the database only contains results of tests conducted on natural soils, mainly consisting of clays and silts with just a few sandy samples. The latter are characterized however by a not negligible fine content. Consequently, the analysis is performed with reference to empirical models suitable for predicting

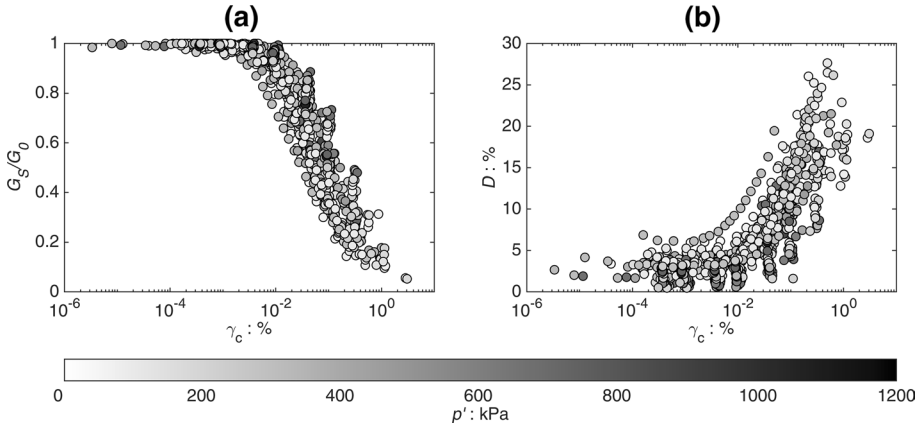

Fig. 11 Modulus reduction (**a**) and damping ratio (**b**) curves for soils with $15\% < PI < 25\%$ as a function of p'

the response of fine-grained soils. In particular, the models here considered are those proposed by: (1) Vucetic and Dobry (1991); (2) Darendeli (2001); (3) Ciancimino et al. (2020); and (4) Wang and Stokoe (2022).

All these models take into account the dependency of the MRD curves on the soil plasticity, but some also consider the influence of other parameters defining the soil material as well as the loading conditions. In addition, also the mathematical structure of the equations adopted to describe the MRD curves varies from model to model. A summary of the main equations is presented in Table 1 along with the input parameters required to predict the nonlinear soil behaviour. A brief description of the structure of each model is provided in "Appendix 2".

The statistical analysis is performed referring to a subset of the database composed of tests for which all the required input parameters are available, namely: PI, FC, OCR, e, w_n, f, and p'. It is worth mentioning that the Darendeli (2001) model also includes the number of loading cycles N as a parameter influencing the damping ratio curves. Within this study, its minor (especially in the medium strain range) influence was however neglected by adopting $N = 10$, as it is not straightforward to define N for a RC test. Moreover, only plastic soils with a fine content $FC > 12\%$ are included, considering that the tested empirical models have been specifically developed to study the response of fine-grained soils. The tests originally used to calibrate the model by Ciancimino et al. (2020) are also excluded from the subset to guarantee the reliability of the statistical analysis. The independence of the regression models from the experimental data used for the verification is indeed crucial to properly assess their predictive capabilities.

The subset for the statistical analysis includes eventually 99 tests (49 RC and 50 CDS-DSS tests) conducted on samples with PI ranging from 6 to 53%. The details of the experimental data used for the statistical analysis are given in "Appendix 1".

4.1 Modulus reduction curve

The comparison between measured and predicted G_S/G_0 values is presented in Fig. 12 for the four empirical models. The figure also reports the R^2 values associated with each model, computed as:

Table 1 Summary of model equations and parameters

Empirical model		D_0	$G_s/G_0 - \gamma_c$	$D - \gamma_c$	Input parameters
Vucetic and Dobry (1991)		Not given	Charts	Charts	PI
Darendeli (2001)*		$D_0 = \left(0.8005 + 0.0129 \cdot PI \cdot OCR^{-0.1069}\right) \cdot p'^{-0.2889} \cdot (1 + 0.2919 \cdot \ln(f))$	$G_s/G_0 = \frac{1}{1+\left(\gamma_c/\gamma_r\right)^a}$ $a = 0.919$ $\gamma_r = \left(0.0352 + 0.001 \cdot PI \cdot OCR^{0.3246}\right) \cdot p'^{0.3483}$	$D = b \cdot \left(G/G_0\right)^{0.1} \cdot D_{Masing} + D_0$ $b = 0.6329 - 0.0057 \cdot \ln(N)$	PI, OCR, p', f, N
Ciancimino et al. (2020)*		$D_0 = (1.2808 + 0.0361 \cdot PI) \cdot p'^{-0.2740} \cdot (1 + 0.1340 \cdot \ln(f))$	$G_s/G_0 = \frac{1}{1+\left(\gamma_c/\gamma_r\right)^a}$ $a = 0.9640$ $\gamma_r = (0.0331 + 0.0014 \cdot PI) \cdot p'^{0.1254}$	$D = b \cdot \left(G/G_0\right)^{0.1} \cdot D_{Masing} + D_0$ $b = 0.5062$	PI, p', f
Wang and Stokoe (2022)**	Clayey soils $FC > 12\%$ $PI > 0\%$	$D_0 = 4.86 \cdot (1.99 + FC)^{-1.91 \cdot e - 6.5 \cdot PI} \cdot \left(1 + 106.75 \cdot PI^{1.64}\right) \cdot \left(p'/p_{atm}\right)^{-0.19} + (0.46 \cdot PI)^{1.73 - 1.34 \cdot e}$	$G_s/G_0 = \frac{1}{\left(1+\left(\gamma_c/\gamma_{mr}\right)^a\right)^b}$ $a = 0.896 + 0.412 \cdot FC + 0.534 \cdot PI$ $b = 0.586 - 0.098 \cdot e - 0.135 \cdot FC$ $\gamma_{mr} = (0.02 \cdot e - 0.004 \cdot FC) \cdot \left(p'/p_{atm} + 0.42 \cdot OCR\right)^{0.447 - 0.27 \cdot PI}$	$D = \frac{d \cdot \left(\gamma_c/\gamma_D\right)^c + D_0}{\left(\gamma_c/\gamma_D\right)^c + 1}$ $c = (1.91 \cdot FC)^{1.62 \cdot PI}$ $d = 21.7\%$ $\gamma_D = 0.11 \cdot \left(0.12 \cdot p'/p_{atm} + 5.29 \cdot w_n - FC\right)^{1.45 - PI + w_n - 1.09 \cdot FC}$	p', e, w_n, FC, PI, OCR

*With PI in percentage and p' in atm

**With PI, FC, and w_n in decimals

$$R^2 = 1 - \left[\sum_{i=1}^{n} \left(Y_i - \hat{Y}_i \right)^2 \Big/ \sum_{i=1}^{n} \left(Y_i - \overline{Y} \right)^2 \right] \tag{8}$$

being Y_i and $\hat{Y}_i$ respectively the measured and predicted values of the ith dependent variable (G_S/G_0 in this case), and $\overline{Y}$ the observed average variable.

The R^2 is a statistical measure of the goodness-of-fit of the models which indicates how much variation is explained by the independent variables adopted in the regression. Consequently, it is a proper index of the performance of a model in predicting a given dependent variable.

By looking at the results, it is evident that the comparison is acceptable for practically all the models (Fig. 12). The Wang and Stokoe (2022) equation along with the Vucetic and Dobry (1991) charts are characterized by the highest $R^2 = 0.91$, giving therefore the best

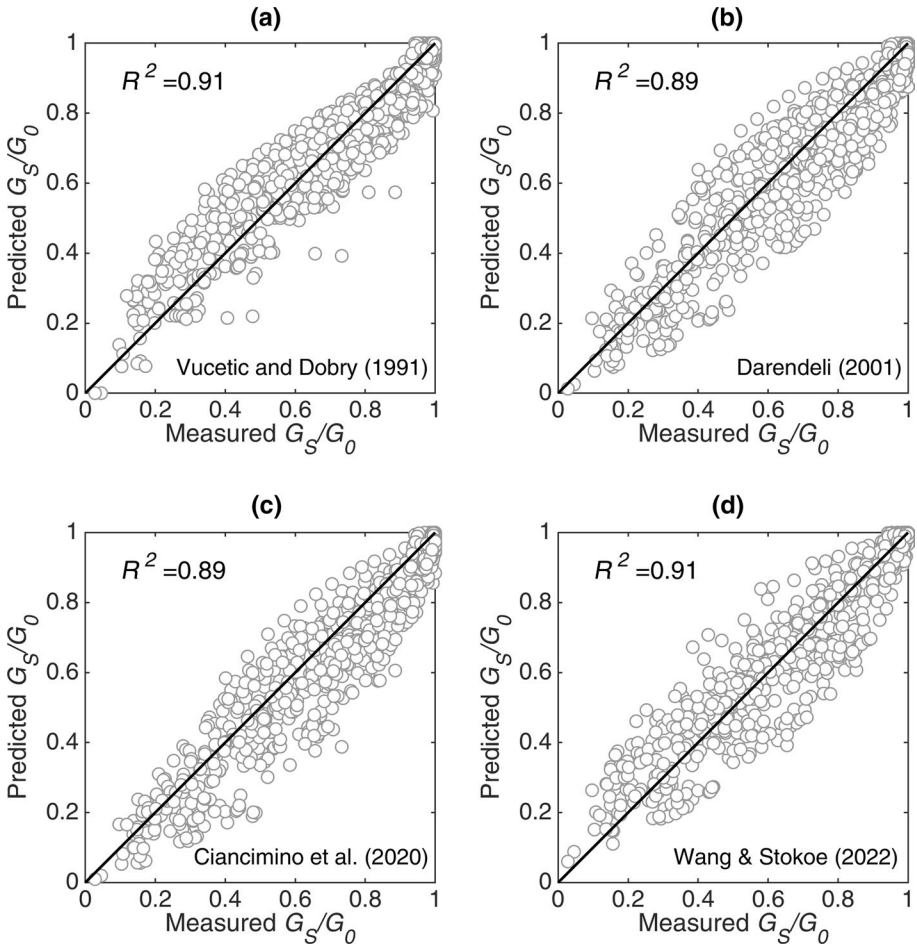

Fig. 12 Comparison between measured and predicted modulus reduction G_S/G_0 curves computed according to: **a** Vucetic and Dobry (1991); **b** Darendeli (2001); **c** Ciancimino et al. (2020); and **d** Wang and Stokoe (2022)

prediction of the G_S/G_0 curves for the investigated soils (Fig. 12a-d). Interestingly, despite their simplicity, the Vucetic and Dobry (1991) charts are effective in predicting the G_S/G_0 curves of fine-grained soils (Fig. 12a). The small differences observed for the Darendeli (2001) and Ciancimino et al. (2020) models can partially be explained by referring to two minor biases which take place in the small-strain field, close to the linearity threshold γ_{tl}, and in the very large strain range. As pointed out by Wang and Stokoe (2022), these two misfit ranges are due to the single curvature modified hyperbolic relationship—Eq. (11) in "Appendix 2"—adopted by the two models to describe the G_S/G_0 curves. The use of such a relationship results indeed in a slight underprediction of G_S/G_0 at small strains and a faster decay at very large strains. Conversely, the double curvature equation proposed by Wang and Stokoe (2022)—Eq. (13) in "Appendix 2"—seems to better capture these strain fields (Fig. 12d). Nevertheless, such biases have a practically negligible effect on the overall performance of the empirical relationships, which are therefore both characterized by R^2 equal to 0.89.

The small-strain misfit can however become significant in problems involving the soil response in the proximity of γ_{tl}. Direct visualization of the issue is given in Fig. 13, which shows the comparison between measured and predicted γ_{tl} values, with the latter being defined as γ_c corresponding to $G_S/G_0 = 0.99$ (Vucetic 1994). The Vucetic and Dobry (1991) model predicts four γ_{tl} values, corresponding to the four curves describing the PI range investigated in the tests (i.e. from 0% to about 50%). The predicted values are generally in good accordance with the experimental ones (Fig. 13a). The Darendeli (2001) and Ciancimino et al. (2020) models instead systematically underpredict γ_{tl}, providing values in a quite narrow range comprised between $2 \bullet 10^{-4}$% and 10^{-3}% (Fig. 13b, c). Conversely, the threshold is well-captured by the double curvature equation adopted by Wang and Stokoe (2022), which guarantees a larger degree of flexibility (Fig. 13d).

4.2 Small-strain damping ratio

An accurate prediction of D_0 is necessary to evaluate the soil response at small strains. Its evaluation is however quite problematic, given its intrinsic variability (Foti et al. 2021). Figure 14 shows the performance of the models in predicting D_0, differentiating the experimental data according to the laboratory which performed the test, and, in turn, the type of test conducted. The measured D_0 values are influenced by the different frequency range applied in RC or CDSDSS tests (Shibuya et al. 1995; d'Onofrio et al. 1999).

For the Vucetic and Dobry (1991) model a constant value, equal to 1%, is used as predicted value, resulting in a systematic underprediction of D_0 (Fig. 14a). Such a value derives from the discretization of the charts, as commonly adopted in software for site response analyses—namely Deepsoil 7 (Hashash et al. 2020) and Strata (Kottke and Rathje 2019). The Authors however originally plotted a dashed zone in the charts due to insufficient experimental data in the small-strain field, mentioning a range of measured values varying from 0.5% to about 5.5%. EPRI (1993) and Lanzo and Vucetic (1999) subsequently clarified the dependency of D_0 from PI, which is responsible for the cross-over shear strain of the D curves (Fig. 9b).

The Darendeli (2001) relationship for D_0 explicitly considers the influence of f, additionally to PI, p' and OCR (Table 1). The effect of f does not seem to be well-captured by the model, inducing a significant underestimation of D_0 for the experimental data coming from CDSDSS tests (Fig. 14b), typically conducted at $f \approx 0.25$Hz. A similar empirical relationship is also adopted by Ciancimino et al. (2020). The Authors however evaluated

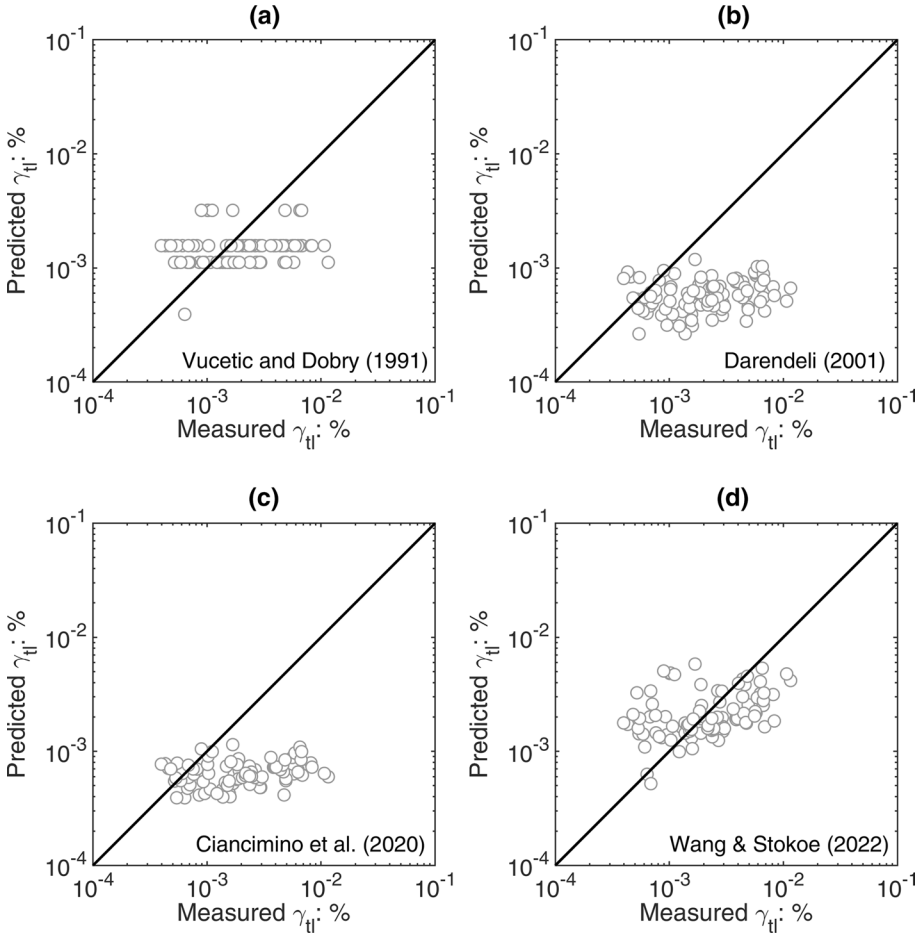

Fig. 13 Comparison between measured and predicted linear threshold shear strains γ_{tl} computed according to: **a** Vucetic and Dobry (1991); **b** Darendeli (2001); **c** Ciancimino et al. (2020); and **d** Wang and Stokoe (2022)

the calibration parameters considering, in the original dataset, also D_0 values measured at small frequencies. Therefore, the predictions given by the model are satisfying both for RC and CDSDSS tests (Fig. 14c). Finally, the equation for D_0 proposed by Wang and Stokoe (2022) does not consider f as a parameter (Table 1), while it includes several additional soil parameters (e.g. e, w_n, and FC). Data coming from low-frequency cyclic tests are then frequently overpredicted by the model, as shown in Fig. 14d.

4.3 Damping ratio curve

The performances of the models in predicting the measured D curves are shown in Fig. 15, which also reports the R^2 values. The prediction of the D curves is more complex

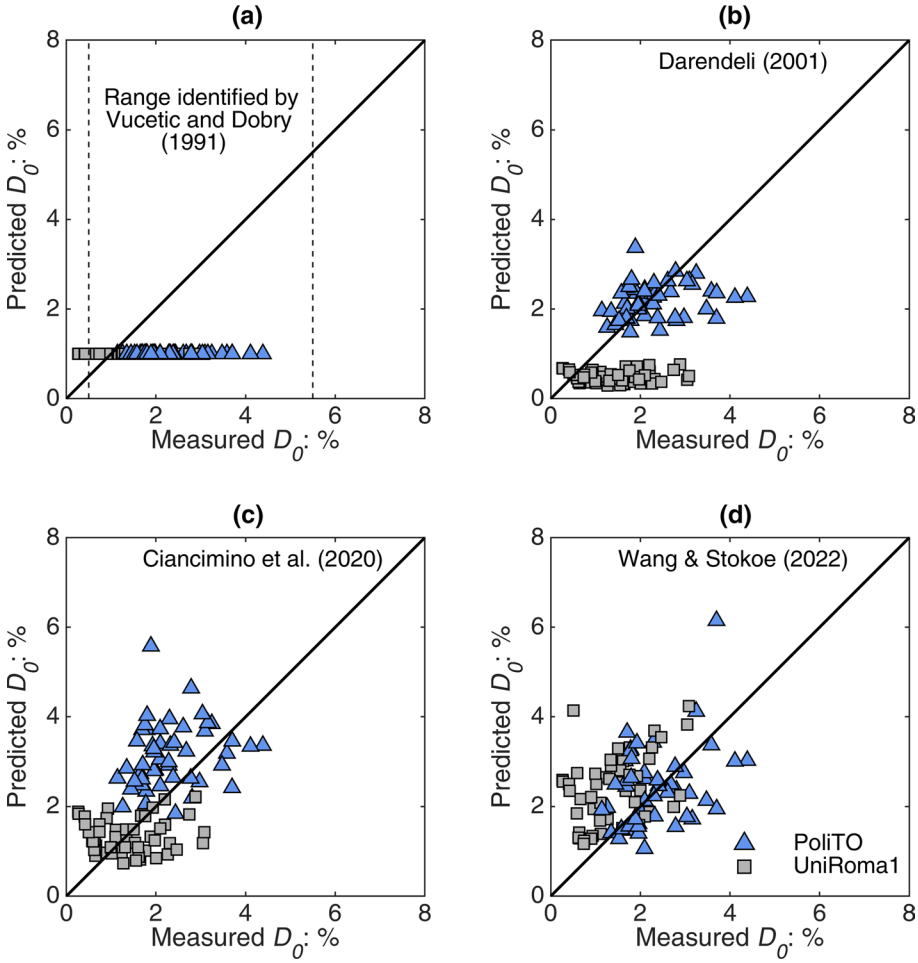

Fig. 14 Comparison between measured and predicted small-strain damping ratios D_0 computed according to: **a** Vucetic and Dobry (1991); **b** Darendeli (2001); **c** Ciancimino et al. (2020); and **d** Wang and Stokoe (2022)

concerning the G_S/G_0 curves. Consequently, the observed R^2 are significantly lower than the ones obtained for G_S/G_0, ranging from 0.67 to 0.76 (Fig. 12).

By looking more in-depth into the different models, it can be observed that the Vucetic and Dobry (1991) charts show the lowest R^2 value, equal to 0.67 (Fig. 15a). Such a poor prediction is strongly influenced by the assumed constant D_0 value, which appears to be relatively low. The performance of the other models is instead quite similar, with $R^2 = 0.74 \div 0.76$ (Fig. 15b–d). The models are however characterized by different structures. The Darendeli (2001) model links D to G_S/G_0—Eq. (12) in "Appendix 2"—as a function of a calibration parameter depending on N. Conversely, Wang and Stokoe (2022) provide a relationship—Eq. (14) in "Appendix 2"—that depends on several soil properties (i.e. p', e, w_n, FC, PI, and OCR) according to the soil type considered. Finally, Ciancimino et al. (2020) adopted the same approach proposed by Darendeli (2001) but neglected the influence of N on the calibration parameter. The latter provides the best estimation for the

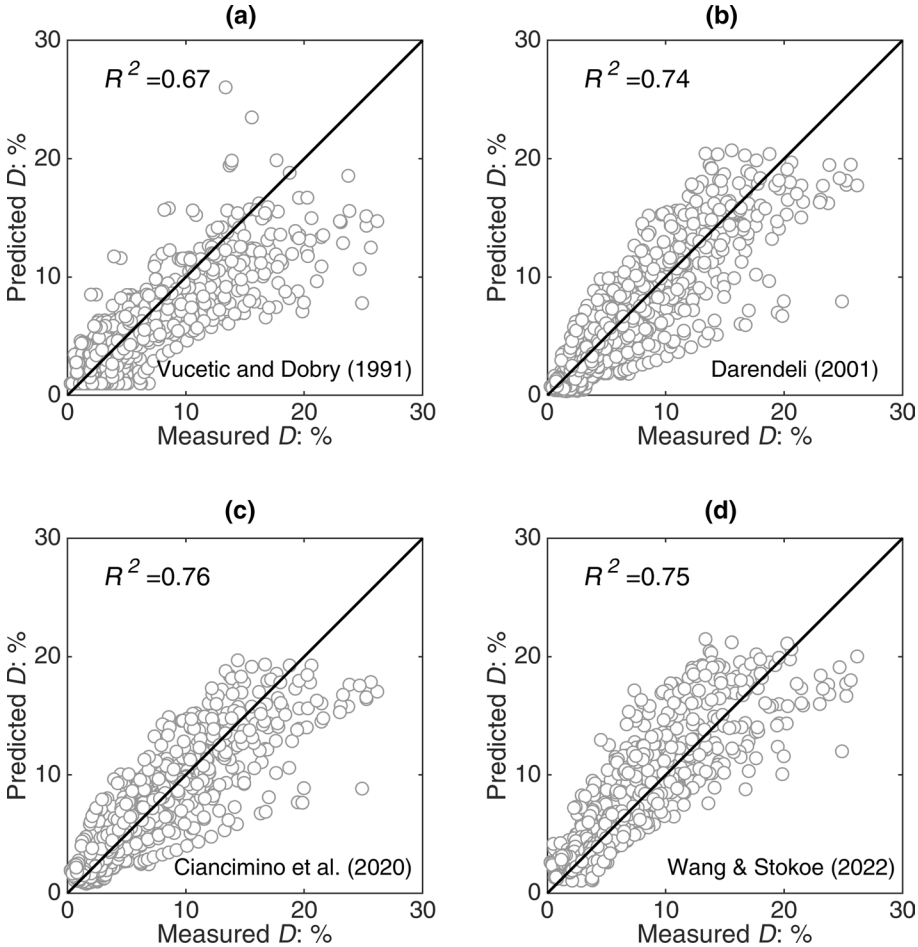

Fig. 15 Comparison between measured and predicted damping ratio D curves computed according to: **a** Vucetic and Dobry (1991); **b** Darendeli (2001); **c** Ciancimino et al. (2020); and **d** Wang and Stokoe (2022)

D curves, with $R^2 = 0.76$ (Fig. 15c), probably also as a result of the good prediction provided by the relationship suggested for D_0 (Fig. 14c).

4.4 Discussion

The R^2 is a good indicator to evaluate the ability of an empirical model in predicting a specific dependent variable. However, to assess the overall performance of the models it is useful to define a unique, normalized, indicator. To this end, the global normalized root-mean-square error $\overline{\varepsilon}$ for each model is computed as:

$$\overline{\varepsilon} = \sqrt{\overline{\varepsilon}^2_{G_S/G_0} + \overline{\varepsilon}^2_D} \tag{9}$$

where $\overline{\varepsilon}_{G_S/G_0}$ and $\overline{\varepsilon}_D$ are the normalized root-mean-square errors respectively for G_S/G_0 and D, obtained as:

$$\overline{\varepsilon}_{G_S/G_0 \text{or} D} = \sqrt{\frac{\sum_{i=1}^{n}\left(Y_i - \hat{Y}_i\right)^2}{n}} \cdot \frac{1}{\overline{Y}} \tag{10}$$

The results are presented in Table 2. The specific errors $\overline{\varepsilon}_{G_S/G_0}$ and $\overline{\varepsilon}_D$ are consistent with the observed R^2 values: the predictions are generally satisfying in terms of G_S/G_0 curves while the models struggle in predicting the D curves. As a consequence, the performances of the models are strongly influenced by the D predictions when looking at the global error $\overline{\varepsilon}$. The Vucetic and Dobry (1991) model is thus characterized by the largest value ($\overline{\varepsilon} = 0.47$), while the best performance is shown by the Ciancimino et al. (2020) and Wang and Stokoe (2022) models with $\overline{\varepsilon} = 0.41$. Finally, the Darendeli (2001) model presents $\overline{\varepsilon}$ value equal to 0.42.

It is interesting to notice that the computed errors for the different models are very close one each other. For instance, although the double curvature equation adopted by Wang and Stokoe (2022) has proven to be effective in reducing the prediction biases on the G_S/G_0 curves (Fig. 12), the corresponding $\overline{\varepsilon}_{G_S/G_0}$ is not substantially lower than the other models (Table 2). At the same time, for the same model, the use of several soil parameters does not lead to a substantial improvement of $\overline{\varepsilon}_D$, which is instead slightly larger than the value obtained through the relationship proposed by Ciancimino et al. (2020), based just on a few parameters. This suggests that the introduction of further soil parameters as proxies for the MRD curves does not necessarily imply a reduction of the associated uncertainties. Such a result is particularly important given the *independence* of the tested models on the experimental dataset. Indeed this is the most robust (and perhaps the only) way to assess if the introduction of more complicated relationships would lead to an improvement of the model predictions or not.

5 Conclusions

This paper has presented a wide, comprehensive, database of cyclic and dynamic laboratory tests on natural Italian soils. The experimental data include the main physical properties of the investigated soils along with the results of 110 RC and 142 CDSDSS tests conducted, respectively, by the geotechnical laboratories of the Politecnico di Torino and the *Sapienza* Università di Roma. The database is made publicly available as supplementary data for this paper, and it represents a valuable resource for both scientific studies on nonlinear soil behaviour and more practical applications related to site response analyses.

Table 2 Normalized root-mean-square errors of the empirical predictive models

Empirical model	$\overline{\varepsilon}_{G_S/G_0}$	$\overline{\varepsilon}_D$	$\overline{\varepsilon}$
Vucetic and Dobry (1991)	0.10	0.46	0.47
Darendeli (2001)	0.11	0.41	0.42
Ciancimino et al. (2020)	0.11	0.39	0.41
Wang and Stokoe (2022)	0.10	0.40	0.41

The database was then used to assess the performance of empirical models—specifically the Vucetic and Dobry (1991), the Darendeli (2001), the Ciancimino et al. (2020), and the Wang and Stokoe (2022) models—in predicting the MRD curves of fine-grained soils. A subset of the dataset was selected to this end, excluding both the tests conducted on materials without sufficient available information to apply the models and the tests previously used to calibrate the model by Ciancimino et al. (2020). The *independence* of the empirical models from the experimental data employed to test their performance is indeed a crucial point to conduct a reliable statistical analysis.

The predictions in terms of G_S/G_0 curves are generally satisfying for all the models analyzed. Among the models, the one proposed by Wang and Stokoe (2022), along with the Vucetic and Dobry (1991) charts, have been shown to provide the lowest prediction error. In particular, the Wang and Stokoe (2022) double curvature modified hyperbolic relationship seems to be effective in predicting the soil linearity threshold γ_{tl}, which is quite significant for problems involving small to moderate shear strains. The models are instead less effective in predicting D. The intrinsic uncertainties related to this parameter lead unavoidably to larger prediction errors. The best predictions for D_0 are provided by the equation proposed by Ciancimino et al. (2020), which can predict the experimental data coming from both RC and CDSDSS tests. The best estimate of the D curves is, also in this case, provided by the Ciancimino et al. (2020) model.

The statistical analysis shows that the performance is not significantly different from model to model. Conversely, the number of soil parameters required to predict the MRD curves can vary significantly. For instance, three input parameters—PI, p', and f—are needed to apply the Ciancimino et al. (2020) relationships, with just PI as physical soil property. Conversely, the applicability of the last-stage Wang and Stokoe (2022) model requires the estimation of several parameters—p', e, w_n, FC, PI, and OCR—some of them not frequently available. As a consequence, practitioners may be induced to estimate such parameters through empirical correlations, introducing further uncertainties in the evaluation of the MRD curves. When dealing with models to be used in common practice, not only the performance but also the user-friendliness of the developed framework should be considered. It is therefore advisable to find a good balance between the applicability and accuracy of the models, as complexities in applying the model equations may induce a reduction in the reliability of the predictions.

Appendix 1: Summary of the compiled database

Sample ID	Latitude: °	Longitude: °	Depth: m	Soil material	*PI*: %	p' or σ_v': kPa
001_UNIROMA1	42.617	13.167	3.8	Silty sand (SM)	0.0	101
002_POLITO	44.683	7.367	16.4	Silty sand (SM)	0.0	160
003_POLITO	44.683	7.367	8.6	Silty sand with gravel (SM)	0.0	98
004_UNIROMA1	42.327	13.407	6.0	–	0.0	90
005_UNIROMA1	42.327	13.407	6.0	–	0.0	200
006_UNIROMA1	42.327	13.407	6.0	–	0.0	400
007_UNIROMA1	42.322	13.539	0.5	–	0.0	100
008_UNIROMA1	42.322	13.539	0.5	–	0.0	200

Sample ID	Latitude: °	Longitude: °	Depth: m	Soil material	*PI*: %	p' or σ_v': kPa
009_UNIROMA1	42.322	13.539	0.5	–	0.0	400
010_UNIROMA1	44.881	11.331	15.5	–	0.0	100
011_UNIROMA1	44.881	11.331	15.5	–	0.0	200
012_UNIROMA1	44.881	11.331	15.5	–	0.0	400
013_UNIROMA1	44.881	11.331	15.3	–	0.0	100
014_UNIROMA1	44.881	11.331	15.3	–	0.0	200
015_UNIROMA1	44.881	11.331	15.3	–	0.0	400
016_UNIROMA1	44.881	11.331	40.2	–	0.0	180
017_UNIROMA1	44.881	11.331	40.2	–	0.0	360
018_POLITO	44.672	10.926	8.3	Silty sand (SM)	2.7	80
019_POLITO	44.806	10.437	8.0	Silt (ML)	3.6	150
020_POLITO*	44.417	7.917	27.5	Silty, clayey sand (SC-SM)	5.7	251
021_POLITO	42.971	13.587	2.8	Sandy lean clay (CL)	7.9	60
022_POLITO	44.650	10.930	5.8	Sandy lean clay (CL)	8.8	78
023_POLITO*	47.000	11.500	21.8	Lean clay with sand (CL)	8.9	225
024_POLITO*	44.420	7.920	15.9	Lean clay with sand (CL)	9.0	168
025_UNIROMA1	41.888	12.489	36.8	Sandy lean clay (CL)	9.0	600
026_UNIROMA1	42.400	12.860	15.3	Lean clay (CL)	9.6	101
027_UNIROMA1*	41.888	12.489	16.9	Silt (ML)	10.0	280
028_UNIROMA1*	41.888	12.489	16.9	Silt (ML)	10.0	500
029_POLITO	44.820	7.220	62.6	Silt (ML)	10.2	600
030_UNIROMA1*	41.895	12.503	44.5	Lean clay (CL)	11.0	520
031_UNIROMA1*	41.895	12.503	44.5	Lean clay (CL)	11.0	1000
032_UNIROMA1*	41.895	12.503	44.5	Lean clay (CL)	11.0	1500
033_UNIROMA1	42.369	13.343	10.5	Sandy silt (ML)	11.0	160
034_UNIROMA1	42.369	13.343	10.5	Sandy silt (ML)	11.0	320
035_POLITO*	44.370	7.850	4.1	Lean clay with sand (CL)	11.0	78
036_POLITO	44.672	10.926	24.4	Sandy lean clay (CL)	11.9	233
037_POLITO	44.255	9.831	1.3	Clayey sand (SC)	11.9	22
038_POLITO*	44.950	11.420	4.5	Lean clay (CL)	12.0	60
039_UNIROMA1	42.352	14.169	49.3	Lean clay with sand (CL)	12.0	500
040_UNIROMA1	42.352	14.169	49.3	Lean clay with sand (CL)	12.0	1000
041_UNIROMA1*	42.352	14.169	49.3	Lean clay with sand (CL)	12.0	940
042_UNIROMA1	42.520	13.130	5.3	Sandy lean clay (CL)	12.9	80
043_UNIROMA1*	43.723	10.394	6.4	Lean clay with sand (CL)	12.9	66
044_UNIROMA1*	43.723	10.394	6.4	Lean clay with sand (CL)	12.9	131
045_UNIROMA1*	43.723	10.394	6.4	Lean clay with sand (CL)	12.9	262
046_POLITO	44.820	7.220	33.3	Silt (ML)	13.0	533

Sample ID	Latitude: °	Longitude: °	Depth: m	Soil material	*PI*: %	p' or σ_v': kPa
047_POLITO	44.820	7.220	15.3	Silt (ML)	13.4	192
048_POLITO*	43.723	10.397	25.2	Lean clay (CL)	14.0	158
049_UNIROMA1	42.328	13.358	12.0	–	14.0	380
050_UNIROMA1	42.328	13.358	12.0	–	14.0	800
051_UNIROMA1	42.850	13.580	5.8	Sandy lean clay (CL)	14.7	101
052_POLITO*	44.420	7.920	3.3	Sandy lean clay (CL)	14.8	58
053_POLITO	44.520	11.240	37.8	Lean clay (CL)	14.9	380
054_POLITO	36.891	15.071	9.0	–	15.0	167
055_UNIROMA1	36.893	15.069	9.0	–	15.0	167
056_UNIROMA1*	42.328	13.479	49.7	Elastic silt (MH)	16.0	500
057_UNIROMA1*	42.328	13.479	49.7	Elastic silt (MH)	16.0	1000
058_UNIROMA1*	41.888	12.489	45.2	Lean clay (CL)	16.0	660
059_UNIROMA1*	41.888	12.489	45.2	Lean clay (CL)	16.0	1100
060_UNIROMA1*	41.888	12.489	45.2	Lean clay (CL)	16.0	1600
061_UNIROMA1*	41.888	12.489	16.4	Lean clay (CL)	16.0	250
062_UNIROMA1	42.600	13.060	6.8	Silt with sand (ML)	16.1	120
063_POLITO*	41.850	12.470	3.3	Sandy lean clay (CL)	16.4	33
064_POLITO	42.820	13.630	11.8	Sandy lean clay (CL)	16.8	199
065_POLITO	42.770	13.410	3.3	Sandy lean clay (CL)	17.0	60
066_UNIROMA1	42.730	12.730	16.7	Lean clay with sand (CL)	17.0	285
067_UNIROMA1	41.983	12.653	12.3	Lean clay (CL)	17.0	300
068_UNIROMA1	42.696	13.244	6.0	Lean clay (CL)	17.0	120
069_UNIROMA1	42.560	13.370	4.8	Lean clay with sand (CL)	17.7	200
070_UNIROMA1	42.560	13.370	4.8	Lean clay with sand (CL)	17.7	63
071_POLITO*	43.723	10.397	23.7	Silt (ML)	18.0	125
072_POLITO	43.030	13.580	33.8	Lean clay (CL)	18.4	349
073_POLITO*	44.950	11.420	20.8	Silt (ML)	19.0	169
074_UNIROMA1	42.328	13.358	7.0	–	19.0	120
075_UNIROMA1	42.328	13.358	7.0	–	19.0	250
076_UNIROMA1	42.366	13.457	12.0	–	19.0	220
077_UNIROMA1	42.366	13.457	12.0	–	19.0	500
078_UNIROMA1	42.366	13.457	12.0	–	19.0	750
079_UNIROMA1	42.369	13.343	3.3	Sandy lean clay (CL)	19.0	57
080_UNIROMA1	42.369	13.343	3.3	Sandy lean clay (CL)	19.0	110
081_UNIROMA1	42.369	13.343	3.3	Sandy lean clay (CL)	19.0	220
082_UNIROMA1	42.440	13.820	9.5	–	19.1	200
083_POLITO*	47.000	11.500	29.7	Lean clay with sand (CL)	19.3	282
084_POLITO*	44.370	7.850	3.2	Lean clay (CL)	19.4	62
085_UNIROMA1	42.580	12.770	7.8	Lean clay (CL)	19.4	101
086_POLITO*	37.900	13.817	21.8	Clayey sand (SC)	19.7	297
087_POLITO	42.940	13.340	5.3	Sandy lean clay (CL)	20.0	110
088_POLITO	36.891	15.071	13.0	–	20.0	197
089_POLITO	37.508	15.080	35.5	–	20.0	374

Sample ID	Latitude: °	Longitude: °	Depth: m	Soil material	*PI*: %	p' or σ_v': kPa
090_POLITO*	44.900	10.550	5.5	Lean clay (CL)	20.6	82
091_POLITO	42.980	13.690	11.6	Lean clay (CL)	20.6	231
092_UNIROMA1	42.620	12.790	36.3	Lean clay (CL)	20.6	300
093_POLITO	44.672	10.926	40.3	Lean clay (CL)	20.8	399
094_POLITO*	43.723	10.397	15.9	Lean clay (CL)	21.0	138
095_UNIROMA1*	41.888	12.489	28.7	Lean clay (CL)	21.0	510
096_UNIROMA1*	41.888	12.489	28.7	Lean clay (CL)	21.0	1100
097_POLITO	42.940	13.620	11.7	Lean clay with sand (CL)	21.7	199
098_POLITO	36.891	15.071	22.5	–	22.0	301
099_POLITO*	42.887	12.924	6.2	Elastic silt with sand (MH)	22.0	116
100_UNIROMA1	38.273	16.220	14.5	Lean clay (CL)	22.0	275
101_UNIROMA1	38.273	16.220	14.5	Lean clay (CL)	22.0	650
102_UNIROMA1	38.273	16.220	14.5	Lean clay (CL)	22.0	1300
103_UNIROMA1	41.888	12.489	18.9	–	22.0	310
104_UNIROMA1	41.888	12.489	18.9	–	22.0	500
105_POLITO	42.550	13.720	15.3	Lean clay (CL)	22.1	298
106_UNIROMA1	41.895	12.503	55.2	Lean clay (CL)	23.0	400
107_UNIROMA1	41.895	12.503	55.2	Lean clay (CL)	23.0	600
108_UNIROMA1	41.895	12.503	55.2	Lean clay (CL)	23.0	800
109_UNIROMA1*	42.194	13.461	75.3	Fat clay (CH)	23.0	200
110_UNIROMA1*	42.194	13.461	75.3	Fat clay (CH)	23.0	400
111_UNIROMA1*	42.194	13.461	75.3	Fat clay (CH)	23.0	800
112_UNIROMA1*	41.888	12.489	13.0	Elastic silt (MH)	23.0	500
113_UNIROMA1*	41.888	12.489	13.0	Elastic silt (MH)	23.0	1000
114_POLITO*	41.770	12.600	295.5	Lean clay (CL)	23.2	683
115_POLITO*	41.680	14.970	7.2	Elastic silt (MH)	23.5	155
116_POLITO	42.870	13.710	3.3	Lean clay (CL)	23.5	220
117_POLITO	43.020	13.540	25.8	Lean clay (CL)	24.1	299
118_POLITO*	44.672	10.926	32.3	Lean clay (CL)	24.5	309
119_POLITO*	44.661	10.992	6.6	Lean clay (CL)	24.8	98
120_POLITO	42.960	13.490	1.6	Fat clay (CH)	24.9	100
121_UNIROMA1	42.520	13.250	22.3	Lean clay (CL)	24.9	251
122_UNIROMA1	42.830	13.690	5.7	Lean clay (CL)	25.0	200
123_POLITO*	36.891	15.071	22.2	Lean clay with sand (CL)	25.0	294
124_POLITO*	43.723	10.397	14.9	Lean clay (CL)	25.0	87
125_UNIROMA1	41.892	12.488	41.0	Lean clay (CL)	25.0	500
126_UNIROMA1*	36.893	15.069	22.2	Lean clay with sand (CL)	25.0	294
127_UNIROMA1*	36.893	15.069	22.2	Lean clay with sand (CL)	25.0	600
128_UNIROMA1*	36.893	15.069	22.2	Lean clay with sand (CL)	25.0	900
129_UNIROMA1*	36.893	15.069	22.2	Lean clay with sand (CL)	25.0	1500

Sample ID	Latitude: °	Longitude: °	Depth: m	Soil material	*PI*: %	p' or σ_v': kPa
130_UNIROMA1*	36.893	15.069	22.2	Lean clay with sand (CL)	25.0	900
131_UNIROMA1*	36.893	15.069	22.2	Lean clay with sand (CL)	25.0	294
132_UNIROMA1	42.904	12.900	6.3	Sandy elastic silt (MH)	25.0	116
133_UNIROMA1	42.904	12.900	6.3	Sandy elastic silt (MH)	25.0	139
134_UNIROMA1	42.904	12.900	6.3	Sandy elastic silt (MH)	25.0	175
135_UNIROMA1	42.904	12.900	6.3	Sandy elastic silt (MH)	25.0	250
136_UNIROMA1	42.904	12.900	6.3	Sandy elastic silt (MH)	25.0	500
137_UNIROMA1	41.560	14.666	11.5	–	25.0	140
138_UNIROMA1*	37.906	13.815	31.0	Lean clay with sand (CL)	25.0	340
139_UNIROMA1*	37.906	13.815	31.0	Lean clay with sand (CL)	25.0	680
140_UNIROMA1*	37.906	13.815	31.0	Lean clay with sand (CL)	25.0	1600
141_UNIROMA1*	37.906	13.815	31.0	Lean clay with sand (CL)	25.0	1100
142_UNIROMA1*	37.906	13.815	31.0	Lean clay with sand (CL)	25.0	680
143_UNIROMA1*	37.906	13.815	31.0	Lean clay with sand (CL)	25.0	340
144_POLITO*	44.820	11.310	3.7	Fat clay with sand (CH)	25.2	64
145_POLITO	39.080	17.130	6.3	Lean clay (CL)	25.3	130
146_POLITO	42.660	13.700	6.8	Lean clay (CL)	25.8	100
147_UNIROMA1	42.380	12.950	15.8	Fat clay (CH)	25.9	240
148_POLITO	44.672	10.926	16.3	Lean clay (CL)	26.0	161
149_POLITO*	43.345	12.908	6.4	Fat clay (CH)	26.0	98
150_POLITO*	43.345	12.908	6.4	Fat clay (CH)	26.0	99
151_POLITO*	41.860	12.480	49.2	Lean clay (CL)	26.9	204
152_POLITO	36.891	15.071	15.5	–	27.0	242
153_UNIROMA1*	42.904	12.900	4.3	Elastic silt with sand (MH)	27.0	116
154_UNIROMA1*	42.904	12.900	4.3	Elastic silt with sand (MH)	27.0	139
155_UNIROMA1*	42.904	12.900	4.3	Elastic silt with sand (MH)	27.0	151
156_UNIROMA1*	42.904	12.900	4.3	Elastic silt with sand (MH)	27.0	172
157_UNIROMA1*	42.904	12.900	4.3	Elastic silt with sand (MH)	27.0	250
158_UNIROMA1*	42.904	12.900	4.3	Elastic silt with sand (MH)	27.0	500
159_POLITO	39.080	17.130	9.3	Fat clay (CH)	28.0	142
160_POLITO	39.080	17.130	15.8	Lean clay (CL)	28.0	320
161_POLITO	39.080	17.130	7.3	Lean clay (CL)	28.1	995
162_POLITO	39.080	17.130	9.8	Fat clay (CH)	28.1	132
163_POLITO	39.080	17.130	28.3	Fat clay (CH)	28.3	576
164_POLITO	37.508	15.080	21.8	–	28.6	249

Sample ID	Latitude: °	Longitude: °	Depth: m	Soil material	*PI*: %	p' or σ_v': kPa
165_POLITO*	41.680	14.970	2.3	Fat clay (CH)	29.0	350
166_UNIROMA1	42.114	14.706	0.7	–	29.0	80
167_UNIROMA1	42.114	14.706	0.7	–	29.0	160
168_UNIROMA1	42.114	14.706	0.7	–	29.0	320
169_POLITO	39.080	17.130	20.3	Fat clay (CH)	29.0	270
170_UNIROMA1	42.600	12.770	5.6	Fat clay (CH)	29.1	47
171_POLITO	39.080	17.130	20.3	Fat clay (CH)	29.2	384
172_UNIROMA1	42.400	13.020	3.3	Elastic silt (MH)	29.7	101
173_POLITO*	42.887	12.924	4.2	Elastic silt with sand (MH)	29.8	80
174_POLITO*	43.723	10.397	33.8	Fat clay (CH)	30.0	220
175_UNIROMA1*	42.194	13.461	3.3	Fat clay (CH)	30.0	100
176_UNIROMA1*	42.194	13.461	3.3	Fat clay (CH)	30.0	200
177_POLITO	39.080	17.130	3.8	Fat clay (CH)	30.1	82
178_POLITO	39.080	17.130	29.3	Fat clay (CH)	30.8	592
179_POLITO	39.080	17.130	8.3	Fat clay with sand (CH)	30.9	176
180_POLITO	39.080	17.130	4.3	Fat clay (CH)	30.9	83
181_POLITO	39.080	17.130	9.3	Fat clay (CH)	30.9	186
182_POLITO*	41.680	14.970	11.8	Fat clay (CH)	31.0	398
183_POLITO	44.806	10.437	37.9	Fat clay (CH)	31.0	467
184_POLITO*	43.723	10.397	12.9	Elastic silt (MH)	31.0	111
185_POLITO	39.080	17.130	20.7	Fat clay (CH)	31.0	431
186_POLITO	39.080	17.130	7.4	Fat clay (CH)	31.0	148
187_POLITO	39.080	17.130	22.3	Fat clay (CH)	31.0	281
188_POLITO	37.500	15.070	20.8	Fat clay (CH)	31.1	211
189_POLITO	39.080	17.130	21.3	Fat clay (CH)	31.3	443
190_UNIROMA1	42.530	13.120	5.7	Elastic silt (MH)	31.4	101
191_POLITO	37.508	15.080	38.8	–	31.4	411
192_POLITO*	43.723	10.397	12.7	Elastic silt (MH)	31.6	82
193_POLITO	47.000	11.500	39.3	Fat clay (CH)	31.9	346
194_POLITO	39.080	17.130	21.6	Fat clay (CH)	32.1	450
195_POLITO*	41.680	14.970	14.8	Fat clay (CH)	32.1	397
196_POLITO	39.080	17.130	22.8	Fat clay (CH)	32.2	480
197_POLITO*	43.723	10.397	21.0	Fat clay (CH)	33.0	137
198_POLITO	41.750	14.520	35.1	Fat clay with sand (CH)	33.5	698
199_POLITO*	43.723	10.397	16.9	Fat clay (CH)	34.0	107
200_UNIROMA1	42.730	12.730	19.5	Fat clay (CH)	34.2	300
201_POLITO*	41.850	12.470	30.3	Fat clay (CH)	34.4	299
202_POLITO*	41.850	12.470	64.7	Fat clay (CH)	34.5	702
203_POLITO*	43.723	10.397	29.5	Fat clay (CH)	35.0	194
204_POLITO*	41.850	12.470	46.8	Fat clay (CH)	35.5	498
205_POLITO	42.870	13.710	19.8	Fat clay with gravel (CH)	36.0	248
206_POLITO	36.891	15.071	51.3	–	36.0	521
207_POLITO*	44.950	11.760	20.4	Elastic silt (MH)	36.3	160
208_POLITO*	43.723	10.397	17.5	Fat clay (CH)	37.0	107

Sample ID	Latitude: °	Longitude: °	Depth: m	Soil material	*PI*: %	p' or σ_v': kPa
209_UNIROMA1	42.460	13.230	15.3	Fat clay (CH)	37.0	176
210_POLITO*	41.680	14.970	1.8	Fat clay (CH)	37.6	99
211_POLITO*	43.723	10.397	21.9	Fat clay (CH)	39.0	123
212_UNIROMA1*	41.902	12.462	12.2	Fat clay (CH)	39.0	144
213_UNIROMA1*	41.902	12.462	12.2	Fat clay (CH)	39.0	296
214_UNIROMA1*	41.902	12.462	12.2	Fat clay (CH)	39.0	590
215_UNIROMA1*	41.902	12.462	12.2	Fat clay (CH)	39.0	1200
216_POLITO*	37.240	15.200	12.3	Fat clay (CH)	40.1	235
217_POLITO*	41.860	12.480	19.9	Fat clay (CH)	40.9	101
218_POLITO	44.806	10.437	28.0	Elastic silt (MH)	42.7	339
219_UNIROMA1	37.250	15.222	–	–	43.7	250
220_UNIROMA1	37.250	15.222	–	–	43.7	400
221_UNIROMA1	37.250	15.222	–	–	43.7	1250
222_UNIROMA1	37.250	15.222	–	–	43.7	1670
223_UNIROMA1	37.250	15.222	–	–	43.7	1250
224_UNIROMA1	37.250	15.222	–	–	43.7	800
225_UNIROMA1	37.250	15.222	–	–	43.7	400
226_UNIROMA1	37.250	15.222	–	–	43.7	250
227_UNIROMA1	37.250	15.222	–	–	43.7	400
228_UNIROMA1	37.250	15.222	–	–	43.7	800
229_UNIROMA1	37.250	15.222	–	–	43.7	1250
230_UNIROMA1	37.250	15.222	–	–	43.7	1670
231_UNIROMA1	41.902	12.462	30.0	Fat clay (CH)	45.0	100
232_UNIROMA1	41.902	12.462	30.0	Fat clay (CH)	45.0	200
233_UNIROMA1	41.902	12.462	30.0	Fat clay (CH)	45.0	350
234_UNIROMA1	41.902	12.462	30.0	Fat clay (CH)	45.0	700
235_POLITO	41.750	14.520	6.3	Fat clay with sand (CH)	47.2	100
236_UNIROMA1	37.906	13.815	22.0	–	48.0	264
237_UNIROMA1	37.906	13.815	22.0	–	48.0	500
238_UNIROMA1	37.906	13.815	22.0	–	48.0	750
239_UNIROMA1	37.906	13.815	22.0	–	48.0	1400
240_POLITO*	44.350	10.990	13.3	Elastic silt (MH)	49.0	150
241_UNIROMA1	36.893	15.069	15.5	–	49.0	242
242_POLITO	44.520	11.240	14.8	Fat clay (CH)	49.5	148
243_POLITO*	37.900	13.820	9.3	Fat clay (CH)	49.6	98
244_UNIROMA1	42.381	14.308	51.6	–	50.0	1100
245_UNIROMA1	42.381	14.308	51.6	–	50.0	1100
246_UNIROMA1*	41.926	12.545	32.7	Elastic silt (MH)	50.5	390
247_UNIROMA1*	41.926	12.545	32.7	Elastic silt (MH)	50.5	600
248_UNIROMA1*	41.926	12.545	32.7	Elastic silt (MH)	50.5	800
249_UNIROMA1*	41.926	12.545	32.7	Elastic silt (MH)	50.5	1200
250_POLITO*	44.672	10.926	24.3	Fat clay (CH)	51.4	237
251_POLITO*	43.723	10.397	13.4	Fat clay (CH)	53.0	53
252_POLITO	44.661	10.992	20.1	Sandy elastic silt (MH)	122.4	79

*Data included in the subset employed for the statistical analyses

Appendix 2: Empirical predictive models

The model developed by Vucetic and Dobry (1991) is one of the first, and probably the most used, empirical model for fine-grained soils. The Authors provided representative MRD curves in a chart showing the influence of PI, the only input parameter required, on the material behaviour. The MRD curves have been presented just in graphic form, therefore to test the model capabilities it is adopted the discretization proposed in widely-used codes for site response analyses (Deepsoil 7, Hashash, 2020). For each experimental point obtained for a given γ_c, the model predictions are obtained by linearly interpolating (in a logarithmic scale) the discretized curves corresponding to the PI closest to the one of the sample.

A further step in predicting the MRD curves of fine-grained soils is represented by the Darendeli (2001) regression model, which is based on five input parameters: PI; OCR; p'; f; and N. The model adopts a modified version of the hyperbolic model proposed by Hardin and Drnevich (1972) to describe the G_s/G_0 curve. The classical functional form is modified through a curvature parameter a to improve the fitting of the experimental data:

$$G_s/G_0 = \frac{1}{1 + \left(\gamma_c/\gamma_r\right)^a} \tag{11}$$

where γ_r is the reference shear strain corresponding to $G_s/G_0 = 0.5$, linked to PI, OCR, and p' (Table 1). The D curve is instead obtained by summing up the small-strain D_0 value to the hysteretic D:

$$D = b \cdot \left(G/G_0\right)^{0.1} \cdot D_{Masing} + D_0 \tag{12}$$

The D_0 can be computed as a function of, OCR, p' and f (Table 1). The hysteretic D is instead obtained as a function of G_s/G_0 by modifying the value coming from the application of the Masing (1926) unloading–reloading criteria. Such modification is implemented through a calibration parameter b that depends on the number of cyclic loadings N (Table 1), for which a standard value of 10 is assumed.

Ciancimino et al. (2020) proposed a regression model specifically calibrated on the results of cyclic and dynamic tests conducted within the framework of the Seismic Microzonation studies in Central Italy. The model follows the same structure previously introduced by Darendeli (2001), with just some minor modifications. The single-curvature hyperbolic relationship of Eq. (11) is adopted for the G_s/G_0 curve, with γ_r depending on PI and p'. The equation proposed for D_0 neglects again the influence of OCR. Finally, the D curve is computed by referring to Eq. (12), where the calibration parameter b is assumed to be constant. The model is therefore based just on three input parameters: PI; p'; and f.

The model recently developed by Wang and Stokoe (2022) introduces new features to the classical structure of empirical models. It is based on staged multivariable regression analyses, performed by introducing different variables according to the order of their importance. The G_s/G_0 curve is modelled through a modified hyperbolic model with two curvature parameters a and b:

$$G_s/G_0 = \frac{1}{\left(1 + \left(\gamma_c/\gamma_{mr}\right)^a\right)^b} \tag{13}$$

being γ_{mr} the reference shear strain corresponding to $G_s/G_0 = 0.5^b$. The second curvature parameter b is added to improve the fitting of the experimental data. In particular, Eq. (13) is claimed to better capture the linearity threshold γ_{tl} and the mismatch in the highly non-linear shear strain range. A three-parameter modified hyperbolic model is instead adopted for the D curve:

$$D = \frac{d \cdot \left(\gamma_c/\gamma_D\right)^c + D_0}{\left(\gamma_c/\gamma_D\right)^c + 1} \tag{14}$$

where c and d are model parameters, and γ_D is the reference shear strain for which $D = \left(d + D_0\right)/2$. As opposed to the Darendeli (2001) and Ciancimino et al. (2020) models, the D curve is therefore independent of the G_s/G_0 curve.

The model parameters, as well as the D_0 equation, can be computed according to a combination of soil properties depending on the soil type as proposed by USCS (ASTM International 2017). Table 1 reports the model equations obtained by Wang and Stokoe (2022) for the last-stage models developed for the soil type considered in this research, i.e. clayey materials. According to the model, the MRD curves of clayey soils depend on six parameters: p'; e; w_n; FC; PI; and OCR.

Acknowledgements The authors want to thank all the people who contributed over the years to carry out the experimental tests. In particular, the support of Giovanni Bianchi (Politecnico di Torino, Italy) and Silvano Silvani (Università di Roma "La Sapienza", Italy) for the execution of the laboratory tests and the compiling of the dataset is gratefully acknowledged.

Authors' contribution All authors contributed to the study's conception and design and the data collection. Material preparation and statistical analyses were performed by Andrea Ciancimino. The first draft of the manuscript was written by Andrea Ciancimino and all authors commented on previous versions of the manuscript. All authors read and approved the final manuscript.

Funding Open access funding provided by Politecnico di Torino within the CRUI-CARE Agreement. Partial funding was provided by the ReLUIS Project WP16.1 "Site response analysis and liquefaction" (2022–24), promoted by the Italian Civil Protection Agency.

Data availability All the experimental data included in the database are publicly available as supplementary data for this paper.

Declaration

Conflict of interest The authors have not disclosed any competing interests.

Open Access This article is licensed under a Creative Commons Attribution 4.0 International License, which permits use, sharing, adaptation, distribution and reproduction in any medium or format, as long as you give appropriate credit to the original author(s) and the source, provide a link to the Creative Commons licence, and indicate if changes were made. The images or other third party material in this article are included in the article's Creative Commons licence, unless indicated otherwise in a credit line to the material. If material is not included in the article's Creative Commons licence and your intended use is not permitted by statutory regulation or exceeds the permitted use, you will need to obtain permission directly from the copyright holder. To view a copy of this licence, visit http://creativecommons.org/licenses/by/4.0/.

References

Aimar M, Ciancimino A, Foti S (2020) An assessment of the NTC18 stratigraphic seismic amplification factors. Ital Geotech J 1:5–21. https://doi.org/10.19199/2020.1.0557-1405.005

Anderson DG, Woods RD (1975) Comparison of field and laboratory shear moduli. Paper presented at the In Situ Measurement of Soil Properties, Raleigh, N.C., June 1–4
ASTM International (2017) ASTM D2487-17 Standard practice for classification of soils for engineering purposes (Unified Soil Classification System). ASTM International, West Conshohocken
Bahrampouri M, Rodriguez-Marek A, Bommer JJ (2019) Mapping the uncertainty in modulus reduction and damping curves onto the uncertainty of site amplification functions. Soil Dyn Earthq Eng 126:105091
Bjerrum L, Landva A (1966) Direct simple-shear tests on a Norwegian quick clay. Geotechnique 16:1–20
Cascante G, Vanderkooy J, Chung W (2003) Difference between current and voltage measurements in resonant-column testing. Can Geotech J 40:806–820
Cavallaro A, Lanzo G, Pagliaroli A, Maugeri M, Lo Presti D (2003) A comparative study on shear modulus and damping ratio of cohesive soil from laboratory tests. In: Proceedings of the 3rd international symposium on deformation characteristics of geomaterials, Lisse, The Netherlands, 2003, pp 257–265
Ciancimino A, Lanzo G, Alleanza GA, Amoroso S, Bardotti R, Biondi G, Cascone E, Castelli F, Di Giulio A, d'Onofrio A (2020) Dynamic characterization of fine-grained soils in Central Italy by laboratory testing. Bull Earthq Eng 18:5503–5531
Ciancimino A, Foti S, Lanzo G, Alleanza GA, d'Onofrio A, Amoroso S, Bardotti R, Madiai C, Biondi G, Cascone E, Castelli F, Lentini V, Di Giulio A, Vessia G (2019) Dynamic characterization of fine-grained soils for the seismic microzonation of Central Italy. Paper presented at the 7th international conference on earthquake geotechnical engineering, Rome, June 17–20
D'Elia B, Lanzo G, Pagliaroli A (2003) Small-strain stiffness and damping of soils in a direct simple shear device. In: Engineering NZSfE (ed) Pacific conference on earthquake engineering, Christchurch, New Zealand, 2003
Darendeli MB (1997) Dynamic properties of soils subjected to 1994 Northridge earthquake. University of Texas at Austin
Darendeli MB (2001) Development of a new family of normalized modulus reduction and material damping curves. PhD Dissertation, University of Texas at Austin
Dobry R, Vucetic M (1987) Dynamic properties and seismic response of soft clay deposits. In: Proc. of the Int. Symp. on Geotech. Engrg. of Soft Soils, vol 2, pp 51–86. Sociedad Mexicana de Mecanica de suelos
d'Onofrio A, Silvestri F, Vinale F (1999) Strain rate dependent behaviour of a natural stiff clay. Soils Found 39:69–82
Doroudian M, Vucetic M (1995) A direct simple shear device for measuring small-strain behavior. Geotech Test J 18:69–85
Drnevich V, Hardin B and Shippy D (1978) Modulus and damping of soils by the resonant-column method. In: ASTM International West Conshohocken, PA, USA
Dyvik R, Berre T, Lacasse S, Raadim B (1987) Comparison of truly undrained and constant volume direct simple shear tests. Geotechnique 37:3–10
EPRI (1993) Modeling of dynamic soil properties. Palo Alto, California
Facciorusso J (2021) An archive of data from resonant column and cyclic torsional shear tests performed on Italian clays. Earthq Spectra 37:545–562
Foti S, Aimar M, Ciancimino A (2021) Uncertainties in small-strain damping ratio evaluation and their influence on seismic ground response analyses. In: Latest developments in geotechnical earthquake engineering and soil dynamics. Springer transactions in civil and environmental engineering, Springer, pp 175–213. https://doi.org/10.1007/978-981-16-1468-2_9
Giusti I, Stacul S, Lo Presti D (2021) Use of 1D and 2D seismic response analyses of soil deposits for seismic Microzonation of urban areas in tuscany (Italy). Ital Geotech J 1:42–61. https://doi.org/10.19199/2021.1.0557-1405.042
Hardin BO, Black WL (1968) Vibration modulus of normally consolidated clay. J Soil Mech Found Div 94:353–369
Hardin BO, Drnevich VP (1972) Shear modulus and damping in soils: design equations and curves. J Soil Mech Found Div 98:667–692
Hashash YMA, Musgrove MI, Harmon JA, Ilhan O, Xing G, Numanoglu O, Groholski DR, Phillips CA, Park D (2020) DEEPSOIL 7, user manual board of Trustees of University of Illinois at Urbana-Champaign, Urbana, IL
Ishibashi I, Zhang X (1993) Unified dynamic shear moduli and damping ratios of sand and clay. Soils Found 33:182–191
Jacobsen LS (1930) Steady forced vibration as influenced by damping. Trans ASME-APM 52:169–181
Kishida T (2016) Comparison and correction of modulus reduction models for clays and silts. J Geotech Geoenviron Eng 143:04016110
Kokusho T, Yoshida Y, Esashi Y (1982) Dynamic properties of soft clay for wide strain range. Soils Found 22:1–18

Kottke AR, Wang X, Rathje EM (2019) Strata technical manual. Pacific Earthquake Engineering Research Center, Berkeley, California
Lanzo G, Vucetic M (1999) Effect of soil plasticity on damping ratio at small cyclic strains. Soils Found 39:131–141
Lanzo G, Vucetic M, Doroudian M (1997) Reduction of shear modulus at small strains in simple shear. J Geotech Geoenviron Eng 123:1035–1042
Lanzo G, Pagliaroli A, Tommasi P, Chiocci F (2009) Simple shear testing of sensitive, very soft offshore clay for wide strain range. Can Geotech J 46:1277–1288
Lo Presti DC (1991) Discussion on" threshold strain in Soils". Paper presented at the X ECSMFE on deformation of soils and displacements of structures, Firenze, Italy
Lo Presti DC, Pallara O, Lancellotta R, Armandi M, Maniscalco R (1993) Monotonic and cyclic loading behavior of two sands at small strains. Geotech Test J 16:409–424
Lo Presti DC, Jamiolkowski M, Pallara O, Cavallaro A, Pedroni S (1997) Shear modulus and damping of soils. Geotechnique 47:603–617
Masing G Eigenspannumyen und verfeshungung beim messing. In: Proceedings of the international congresses on theoretical and applied mechanics, 1926, pp 332–335
Matešić L, Vucetic M (2003) Strain-rate effect on soil secant shear modulus at small cyclic strains. J Geotech Geoenviron Eng 129:536–549
Matlab (2020) 9.8.0.1396136 (R2020a) The MathWorks Inc, Natick
Meng J, Rix G (2003) Reduction of equipment-generated damping in resonant column measurements. Géotechnique 53:503–512
Menq F-Y (2003) Dynamic properties of sandy and gravelly soils. The University of Texas at Austin
Mortezaie AR, Vucetic M (2013) Effect of frequency and vertical stress on cyclic degradation and pore water pressure in clay in the NGI simple shear device. J Geotech Geoenviron Eng 139:1727–1737
Mortezaie A, Vucetic M (2016) Threshold shear strains for cyclic degradation and cyclic pore water pressure generation in two clays. J Geotech Geoenviron Eng 142:04016007
Oztoprak S, Bolton M (2013) Stiffness of sands through a laboratory test database. Géotechnique 63:54–70
Pagliaroli A, Lanzo G, Tommasi P, Di Fiore V (2014) Dynamic characterization of soils and soft rocks of the Central Archeological Area of Rome. Bull Earthq Eng 12:1365–1381
Richart FE, Hall JR, Woods RD (1970) Vibrations of soils and foundations. Prentice Hall, Englewood Cliffs, N.J.
Seed HB, Wong RT, Idriss I, Tokimatsu K (1986) Moduli and damping factors for dynamic analyses of cohesionless soils. J Geotech Eng 112:1016–1032
Seed H and Idriss I (1970) Soil moduli and damping factors for dynamic response analyses, Report no. EERC 70-10. Earthquake Engineering Research Center, University of California, Berkeley, California
Senetakis K, Anastasiadis A, Pitilakis K (2015) A comparison of material damping measurements in resonant column using the steady-state and free-vibration decay methods. Soil Dyn Earthq Eng 74:10–13
Shibuya S, Mitachi T, Fukuda F, Degoshi T (1995) Strain rate effects on shear modulus and damping of normally consolidated clay. Geotech Test J 18:365–375
Silver ML, Seed HB (1971) Volume changes in sands during cyclic loading. J Soil Mech Found Div 97(9):1171–1182. https://doi.org/10.1061/JSFEAQ.0001658
Stokoe K and Santamarina JC (2000) Seismic-wave-based testing in geotechnical engineering. Paper presented at the ISRM international symposium
Stokoe K, Hwang S, Lee J-K and Andrus RD (1995) Effects of various parameters on the stiffness and damping of soils at small to medium strains. Paper presented at the pre-failure deformation of geomaterials. Proceedings of the international symposium, 12–14 September 1994, Sapporo, Japan. 2 Vols.
Stoll RD, Kald L (1977) Threshold of dilation under cyclic loading. J Geotech Eng Div 103:1174–1178
Tabata K, Vucetic M (2010) Threshold shear strain for cyclic degradation of three clays. In: 5th international conference on recent advances in geotechnical earthquake engineering and soil dynamics, Missouri University of Science and Technology, San Diego, May 24th–May 29th 2010
Tatsuoka F, Santucci De Magistris F, Hayano K, Koseki J and Momoya Y Some new aspects of time effects on the stress–strain behaviour of stiff geomaterials. In: The geotechnics of hard soils-soft rocks, 2000, pp 1285–1371
Vardanega P, Bolton M (2013) Stiffness of clays and silts: Normalizing shear modulus and shear strain. J Geotech Geoenviron Eng 139:1575–1589
Vucetic M (1994) Cyclic threshold shear strains in soils. J Geotech Eng 120:2208–2228
Vucetic M, Dobry R (1991) Effect of soil plasticity on cyclic response. J Geotech Eng 117:89–107
Wang Y, Stokoe K (2022) Development of constitutive models for linear and nonlinear shear modulus and material damping ratio of uncemented soils. J Geotech Geoenviron Eng 148:04021192
Wang Y-H, Cascante G, Santamarina JC (2003) Resonant column testing: the inherent counter EMF effect. Geotech Test J 26:342–352

Woods RD (1978) Measurement of dynamic soil properties. Paper presented at the ASCE geotechnical engineering division specialty conference, Pasadena, California, June 19–21
Youd TL (1972) Compaction of sands by repeated shear straining. J Soil Mech Found Div 98:709–725
Zhang J, Andrus RD, Juang CH (2005) Normalized shear modulus and material damping ratio relationships. J Geotech Geoenviron Eng 131:453–464

Publisher's Note Springer Nature remains neutral with regard to jurisdictional claims in published maps and institutional affiliations.